Citation of published paper:
Newnham, R.M., Hazell, Z.J., Charman, D.J., Lowe, D.J., Rees, A.B.H., Amesbury, M.J., Roland, T.P., Gehrels, M.J., van den Bos, V., Jara, I.A. 2019. Peat humification records from Restionaceae bogs in northern New Zealand as potential indicators of Holocene precipitation, seasonality, and ENSO. *Quaternary Science Reviews* 218, 378-394.
https://doi.org/10.1016/j.quascirev.2019.06.03610.1016/j.quascirev.2019.06.036

Peat humification records from Restionaceae bogs in northern New Zealand as potential indicators of Holocene precipitation, seasonality, and ENSO

Rewi M. Newnham[1], Zoë J. Hazell[2*], Dan J. Charman[3], David J. Lowe[4], Andrew B.H. Rees[1], Matthew J. Amesbury[3,5], Tom P. Roland[3], Maria Gehrels[6], Valerie van den Bos[1] ,Ignacio A. Jara[7]

[1] *School of Geography, Environment & Earth Sciences, Victoria University of Wellington, PO Box 600 Wellington, New Zealand*
[2] *Historic England, Fort Cumberland, Fort Cumberland Road, Eastney, Portsmouth, Hampshire, PO4 9LD, UK.*
[3]*Geography, College of Life and Environmental Sciences, University of Exeter, Exeter, UK*
[4]*School of Science, University of Waikato, Private Bag 3105, Hamilton, 3240, New Zealand*
[5]*Environmental Change Research Unit (ECRU), Faculty of Biological and Environmental Sciences, University of Helsinki, Finland*
[6]*Environment Department, York University, United Kingdom*
[7] *Centro de Estudios Avanzados en Zonas Áridas (CEAZA), Colina del Pino, La Serena, Chile*

**corresponding author: rewi.newnham@vuw.ac.nz*

ABSTRACT

In comparison with temperature reconstructions, New Zealand proxy records for paleo-precipitation are rare, despite the importance of precipitation in contemporary climate variability and for projected climate impacts. In this study, records of mid-late Holocene palaeomoisture variation were derived for two hydrologically separate ombrotrophic Restionaceae bogs in northern New Zealand, based on peat humification analysis. At each site, three cores were analysed for peat humification, facilitating both intra- and inter-site comparisons. Age models for the six sequences were developed using radiocarbon dating and tephrochronology. Twelve tephras (including six cryptotephras) were recognised, four of which were used to precisely link the two sites and to define start and end points for the records at 7027 ± 170 (Tuhua tephra) and 1718 ± 10 cal. yr BP (Taupo tephra) (2σ-age ranges), respectively. We find individual differences between the six peat humification records at short-term timescales that are presumably due to local site factors, in particular changing vegetation and microtopography, or to changes in the composition of the material analysed. Stronger longer-term coherence is observed between all six records but is attributed to slow anaerobic decay over time because the implied trend towards wetter summers in the late Holocene cannot be corroborated by independent climate proxies. Despite these confounding factors, centennial scale shifts in bog surface wetness are a pervasive feature of all six records with varying degrees of overlap in time that show strong correspondence with El Niño-Southern Oscillation reconstructions from the eastern equatorial Pacific. These results indicate the potential for peat humification records from New Zealand's ombrotrophic bogs to elucidate past climate variability and also demonstrate the importance of developing multiple well-dated profiles from more than one site.

KEYWORDS: peat humification, ENSO, tephrochronology, effective precipitation, Bayesian age modelling

1.0 Introduction

During the past few decades, changes to the hydrological cycle and precipitation patterns across the planet have been linked to short-term (annual to decadal) variability in regional climate modes (e.g.,Wang & Cai, 2013; Hartmann et al., 2013). In extratropical regions of the Southern Hemisphere such as New Zealand, these patterns, in large part, are explained by a shift towards the high-index positive phase of the Southern Annular Mode (SAM; Marshall, 2003; Renwick, 2005; Kidston et al., 2009) and in northern New Zealand by stronger or more frequent El Niño events as part of more variable ENSO cycles (Salinger & Mullan, 1999; Ummenhofer & England, 2007; Gergis & Fowler, 2009). The recent trend in the SAM has been linked both to increases in greenhouse gases and stratospheric ozone depletion (Fogt et al., 2009; Thompson et al., 2011) and may be unprecedented in the last millennium at least (Abram et al., 2014; Jones et al., 2016). However, as the observational record extends for just a few decades, there is an important need to set these projections and the recent observed trend into a longer historical context. As precipitation variability is a primary indicator for both SAM and ENSO in the southern extratropics (Garreaud et al., 2007), the key to reconstructing past variability in these climate modes lies with finding suitable localities, depositional environments, and proxies to reconstruct paleoprecipitation.

New Zealand is well-served in the first two of these three requirements, but with the notable exception of hydroclimate inferences drawn from speleothem stable isotope records (e.g., Williams et al., 2004), there have been only a few attempts to develop other precipitation proxies. Here we explore the potential of peat humification analysis applied at two raised bogs in northern New Zealand for reconstructing past effective precipitation (precipitation minus evapotranspiration). The method has been widely applied in other regions of the world, although some questions have been raised about its suitability as a paleo-precipitation proxy (see section 2.0). Yet to date only two humification studies have been reported from New Zealand, both from sites in the southern South Island (McGlone & Wilmshurst, 1999; Wilmshurst et al., 2002). Nevertheless, there appears to be good potential in this oceanic setting characterised by strong regional differentiation of hydroclimate and an abundance of raised ombrotrophic (rain-fed) bog sites.

We present multiple humification records, linked precisely via tephrochronology and dated using multiple AMS and conventional radiocarbon (^{14}C) ages, from two hydrologically separate ombrotrophic bogs in northern New Zealand, that span the interval ca 7.0–1.7 calendar/calibrated (cal) ka (all ages calibrated in this study are referred to as cal years BP or cal ka). We test the feasibility of northern New Zealand humification records for reconstructing past precipitation at two time scales for the Holocene: (1) decadal-centennial and (2) millennial scales. Within- and between-site replicability and comparison with other paleo-climate records provide a basis for evaluation: coherent humification patterns within and between the two sites and with other records would support the conclusion that they represent regional precipitation patterns.

2.0 Peat humification as a paleoclimate proxy: potential and limitations

Humification of peat deposits is a widely used paleoclimate proxy that extends back to the 19th century in northern Europe (~~Clymo, 1984; Langdon et al., 2012~~; Zaccone et al., 2018). The modern era of climate reconstruction from peat bogs follows the principle that raised mires in particular could provide continuous records of past hydroclimatic change because they are directly coupled with the atmosphere (Aaby & Tauber, 1975; Barber, 1981). The underlying premise is that peat humification is a measure of organic decay that mainly reflects changing paleohydrological conditions in the thin upper layer or acrotelm. This layer experiences seasonal water table fluctuations, determined largely by the balance between precipitation and evapotranspiration, with associated variability in rates of decomposition. In contrast, decomposition proceeds much more slowly in the anaerobic catotelm and so the degree of peat humification is thought to represent the environmental conditions and in particular bog surface wetness (BSW) at the time of peat accumulation (Aaby & Tauber, 1975; Blackford & Chambers, 1993). Building on this important premise, a suite of climate proxies has been developed and applied to Late Quaternary peat archives.

Although there is a sound conceptual basis, questions have been raised about the wider applicability of humification as a paleoclimate proxy (Chambers et al, 2012; Hughes et al., 2012; Zaccone et al., 2018), such questions being supported by studies that reported inconsistencies between humification and other proxy-records of surface wetness in a peat profile (Yeloff & Mauquoy, 2006; Amesbury et al., 2012). One likely issue is that past changes in botanical composition at the core site may have an influence on humification measurements (Chambers et al., 1997; Payne & Blackford, 2008; Hughes et al., 2012). This issue may be compounded by the small sample sized used for measurement. Others have suggested that local topography and geochemical characteristics of the peat may also influence humification values, while some work has questioned the reliability of the colorometric technique itself for determining humification values (Caseldine et al., 2000; Morgan et al., 2005). Amesbury et al. (2012) also challenged the use of composite curves of BSW that combined results from multi-proxy studies. They showed that climate proxies derived from analyses of testate amoebae, plant macrofossils, and peat humification at an ombrotrophic bog from western Sweden were correlated with climate parameters but at different time scales, suggesting that climate-proxy response times and regional variability may be greater than previously hypothesised. In another study from Sweden that used a similar approach to ours, Borgmark & Wastegård (2008) analysed five peat humification records from three ombrotrophic bogs in order to reduce the influence of local fluctuations and extract regional climate signal.

Historically, peatland proxy-climate research has been undertaken mostly in northern Europe, but is becoming more prominent in parts of Asia and North America. In New Zealand, a long history of peatland research extends back to the seminal work of Cranwell and von Post (1936) and has perhaps gained less international recognition than in other areas (the reader is referred to McGlone, 2009, for an account of New Zealand Holocene peat records; see also Davoren, 1978). Nevertheless, climate reconstructions from New Zealand peatlands are being applied increasingly to elucidate hemispheric and global patterns and test postulated climate forcing mechanisms (e.g., Newnham et al., 2012; Turney et al., 2017). The New Zealand work has mostly deployed pollen analysis, sometimes combined with plant macrofossil analysis (e.g., Newnham et al., 1993; 1995a; Ogden et al., 1993; McGlone & Wilmshurst, 1999; Haenfling et al., 2015; Jara et al., 2017), stable isotopes of plant macrofossils (McGlone et al., 2004), or testate amoebae (Wilmshurst et al., 2002). Recent investigations of the stable isotopic composition of New Zealand Restionaceae peat across modern climate gradients also indicate strong potential for these proxies in climate reconstruction (Amesbury et al., 2015a and b). In northern New Zealand, considerable effort has been applied to developing tephrostratigraphic records from peat profiles, both to provide a robust chronostratigraphic framework for correlating sites, for independently dating climate reconstructions, and to help evaluate volcanic history and risk (Lowe et al., 1999, 2008, 2013; Alloway et al., 2004; Gehrels et al., 2006; Newnham et al., 1995a, 1995b; Newnham et al., 1999). Tephrostratigraphy provides a key chronstratigraphical tool in the current study.

3.0 Study sites and regional setting

Two raised, ombrotrophic bogs, ca 55 km apart in the Waikato region, were investigated (Fig. 1). At Kopuatai and Moanatuatua bogs, thick sequences of peat have accumulated on the surface of volcaniclastic alluvial deposits (Hinuera Formation) of the river systems that drained the central North Island volcanic plateau during the last glacial (Selby and Lowe, 1992; Manville and Wilson, 2004; Edbrooke, 2001, 2005). The peat profiles at the two sites span much the same timeframe, and contain similar suites of tephra layers that enable correlation between sequences and help test and constrain ^{14}C age models developed for them. Cored peat deposits extracted from the bogs have been described in a number of earlier studies (de Lange and Lowe 1990; Hodder et al., 1991; Newnham et al., 1995a; Shearer, 1997; Gehrels et al., 2006; Haenfling et al., 2015; Jara et al., 2017) and are summarised in Fig. 2.

**Fig 1 here*

**Fig 2 here*

The vegetation communities growing at both bogs show low plant diversity with only 10−15 common species. Most prominent are two species of the Southern Hemisphere Restionaceae (or restiad) family: *Empodisma robustum* (lesser wire rush) and *Sporadanthus ferrugineus* (greater wire rush or cane rush) (de Lange *et al*., 1999; Wagstaff and Clarkson, 2012), while other common species include *Leptospermum scoparium* (Myrtaceae), the fern *Gleichenia dicarpa,* epacrids *Dracophyllum scoparium* and *Epacris pauciflora*, and several sedges in the genera *Schoenus* and *Baumea*. Sundews *(Drosera)* may be locally common along with *Sphagnum cristatum*. The two restiad species, and in particular *Empodisma,* are the main peat formers and have an essential role in the development of bog environments in this region. Their extensive surface-growing rhizome systems and extremely low evapotranspiration rates enable far greater water retention in a region that experiences frequent summer moisture deficits and therefore is not otherwise considered conducive to peat development (Campbell and Williamson, 1997; Kuder *et al*., 1998; Thompson et al., 1999; Campbell and Jackson, 2004; Ratcliffe *et al*., 2019). The detailed vegetation composition and structure of these bogs were described by Clarkson (2002), Clarkson et al. (2004), and Wagstaff and Clarkson (2012).

Climate of the Waikato region is classed as warm temperate and fully humid (class Cfb as defined in Kottek et al., 2006). In recent decades, annual precipitation has ranged between 1112 and 1500 mm and annual mean temperatures between 13.0 and 14.3 ˚C in lowland regions (Clarkson et al., 2004). Precipitation is stronger in winter (July, ~126 mm) than in summer (February, ~71 mm), and monthly rainfall minima often coincide with the two warmest months, January and February (NIWA, 2009). As a consequence, summer moisture deficits are common at these bogs and typical annual water deficits exceed ~60 mm (Clarkson et al., 2004; Amesbury et al., 2015a&b; Goodrich et al., 2017). Weather conditions (mean air temperature, annual rainfall) across the two sites are broadly similar (Ratcliffe et al., 2019).

3.1. Kopuatai (centre: 37°26'S, 175°34'E)

Kopuatai Bog is an internationally-recognised wetland (Ramsar Site 444) and the largest remaining natural-state peat bog in New Zealand at 18 km long and 10 km wide (Maggs, 1997). It is situated 2–6.5 m above sea level in the Hauraki Depression, a 20-30 km wide rift in the Hauraki lowlands (de Lange & Lowe, 1990; Persaud et al., 2016). Its raised centre is 3 m above the surrounding edges and the maximum peat depth is 12–14 m in central areas (Davoren, 1978; Newnham et al., 1995a). Around ca 7400 cal years BP the northern end of the site was flooded by a marine transgression, directly depositing a thick deltaic mud in the flooded areas and indirectly resulting in the deposition of a minerogenic, freshwater deposit associated with local ponding in the northern area (Newnham et al., 1995a). Two such mud layers were recorded in cores K106 and K204 (Fig. 2). The evolution of the bog and its Holocene vegetation history have been reported previously from pollen, plant macrofossil, and charcoal records (Newnham et al., 1995a).

3.2. Moanatuatua (centre: 37°58'S, 175°72'E)

Situated ~55 km inland and southwest of Kopuatai, Moanatuatua bog was once of similar size, but extensive agricultural drainage schemes since the 1930s have reduced its extent to just 1.1 km^2 (Cranwell, 1939; Clarkson et al., 1999; Thompson *et al*., 1999; Clarkson, 2002; Pronger et al., 2014). The remaining bog, protected as a scientific reserve, is 65 m above sea level, with a peat dome 1–2 m above the surrounding farmland and peat depths reaching 13 m. In the surrounding pasture, farming practices have removed the top 1–2 m of sediment from the edges of the peatland, as demonstrated by the comparison of depths of tephra layers from within and outside the reserve (Shearer, 1997; Schipper and McLeod, 2002). The Holocene vegetation history of Moanatuatua Bog has been shown previously from pollen (Jara et al., 2017) and plant cuticle (Haenfling et al., 2015) records.

4.0 Material and methods

4.1. Fieldwork

At each site, three cores were collected within 300–500 m of one another (Fig. 1) to test replicability between sequences and to develop composite records from multiple cores. Sampling was guided by two prominent tephra layers that were visible in all core sequences (Fig. 2): Tuhua Tephra, c. 7.0 cal ka (Lowe et al., 2013), and Taupo Tephra, c. 1.7 cal ka (Hogg et al., 2012). The humification analyses were confined to the peats in this interval because, below the Tuhua Tephra, marine influence on the Kopuatai hydrology could not be discounted and the near-surface post-Taupo sediments proved in some cases to be too sloppy or fibrous to sample intact. Two other marker tephras were common to both bogs hence further enabling core correlation: Mamaku Tephra, c. 8.0 cal ka and Whakaipo Tephra, c. 2.8 cal ka (see chronology section below). All but one core location were from protected areas, sufficiently far from the drained margins to avoid the likely impacts on peat composition and hydrology (Fig. 1). The exception, core M102, sampled from pastureland adjacent to the Moanatuatua reserve, has a very similar pre-Taupo tephra record to that of the other two cores from this site and so the sediments analysed in this study are unlikely to have been affected by the land use modifications of the past few decades.

All cores were extracted using “Russian”-type D-shaped corers. Core sections were extracted in alternate, overlapping sections from two holes *c.* 1 m apart to avoid gaps and to prevent disturbance of the adjacent, lower-lying sediment by the corer’s pointed nose. Once retrieved, all cores were stored in plastic piping, wrapped in non-PVC clingfilm, and refrigerated at 4^{o}C.

4.2 Laboratory analyses

4.2.1 Core subsampling

The uppermost subsample from each core was taken from the 1 cm section immediately below the Taupo Tephra layer, with subsequent samples extracted down-core at regular intervals. For humification, water content, and total organic carbon analyses, one core from each site (Kopuatai K204 and Moanatuatua M206) was sampled every 2 cm, which represents an estimated between-sample time interval of 20 to 40 years. The other two cores at each site were sampled every 4 cm. Each sub-sample was 1-cm thick due to the fibrous nature of the peat preventing finerresolution subsampling. A suite of analyses was carried out on each sample as described below.

4.2.2 Total organic carbon

Samples were oven-dried overnight then water content was calculated as a percentage of the total wet weight. Total organic carbon (TOC) was measured using a Shimadzu TOC5000 TOC analyser, with the solid sample module-5000A furnace at 900^{o}C. This method was used in preference to loss-on-ignition because of the small amount of sample required for processing. For each sample, three repeat measurements were taken, and averaged. The results were used to correct for mineral content within peat samples, to determine a cut-off point for inclusion in humification analyses as described below, and to assist in determining the positions of cryptotephra deposits in these sequences (Gehrels et al., 2006).

4.2.3 Humification

Peat humification was determined using the colorimetric method based on the light transmission of the alkali-extracted humic acids in solution (Blackford and Chambers, 1993). Light transmission is inversely related to the degree of peat decomposition: the more decomposed or humified the sample, the less light transmitted. The degree of peat humification is largely controlled by moisture level of the near-surface peats, which in ombrotrophic bogs is determined by effective precipitation. Thus light transmission can be used as a proxy for ‘bog wetness’ reflecting the balance of precipitation and evaporation. In this study, following the method of Blackford and Chambers (1993), percentage light transmission was measured at a wavelength of 550 nm on a Zeiss Specord M500 spectrophotometer. For each sample, three readings were taken and the mean value calculated.

Correction for minerogenic content

The relationship between light transmission and peat humification can be distorted in peat samples containing minerogenic constituents, which may be comparatively high in the Waikato peats because of volcanogenic (tephra-fall derived) matter. The presence of some highly minerogenic (tephra, clay) samples made it necessary to determine a cut-off point beyond which light transmission values could not be used confidently to reflect peat humification. In this study, light transmission data for samples with <45% TOC were ignored as these samples corresponded with visible tephra or clay layers. For the remaining (peat-rich) samples with >45% TOC, it was necessary to correct light transmission values for any distortion caused by varying levels of minerogenic matter. Previous work recommended a simple linear correction for this effect based on the minerogenic content determined by LOI (Blackford and Chambers, 1993; Roos-Barraclough et al. 2004; Chambers et al., 2011). Hazell (2004) developed a modified procedure after finding a non-linear relationship between mineral content and light transmission in these Waikato peats. In this study we use the procedure developed by Hazell (2004) to correct for mineral matter based on this non-linear relationship (see Supplementary Information for details).

Detrending for long-term decay effect

Because humification proceeds incrementally with time, it is necessary to consider the possibility that the corrected humification measurements may in part reflect the effects of long-term decay (Clymo, 1984). To counter this possible effect, some workers (e.g., Borgmark and Wastegård, 2008) have presented humification data as normalised and detrended, usually by linear regression with the assumption that long-term anaerobic decay of peat occurs linearly over time. This approach is valid when the goal is solely to investigate shorter term climate 'shifts' but it precludes the possibility of investigating longer term shifts in climate. To allow for this possibility as well, our approach was to present the humification values in both detrended and non-detrended form. We use the detrended data to investigate shorter term climate shifts and the raw corrected (non-detrended) data to consider the possibility of longer term climate trends. We then compare these longer term humification trends with independent climate proxy records from these sites and elsewhere in the region to evaluate whether long-term decay or climate is the more likely controlling factor.

To detrend the data, simple linear regression by age was applied to each humification record and residuals from the regression line were calculated. Both detrended residuals and raw data were normalised to the period between the Tuhua and Taupo tephras (c 7000-1700 cal. yr BP), a period common to all cores.

Correlation of humification records at decadal-centennial scale

We conducted correlation analysis to test for the coherence between the three humification records developed at each site. Using the age models developed, we divided each sequence into 100-year bins and calculated the mean humification value for each bin. We then calculated the Pearson product moment correlation coefficients between each pair of sequences. The associated P values enabled a test of significance for each correlation.

4.3 Chronology

The cores comprised mainly peat with sparse occurrences of small plant macrofossils (or fragments of such material), occasional visible tephra layers each between a few millimetres or centimetres in thickness, and a 30–50 cm clay layer in two cores from Kopuatai (Fig. 2). A combination of tephrochronology and radiocarbon dating was used to derive detailed age-depth models and to correlate cores within and between sites.

4.3.1 Stratigraphy and chronology of tephras

Twelve tephras in total were identified, six as visible layers, five as cryptotephras (glass shard and/or crystal concentrations insufficiently numerous, or too fine, to be visible as a layer to the naked eye: Lowe, 2011), and one (Whakaipo) as a thin layer in one core but as a cryptotephra deposit in others (Fig. 2). All but two of the tephras are rhyolitic in composition and were able to be correlated with characterised and defined equivalent deposits elsewhere; two are andesitic and remain uncorrelated but their compositions indicate that they were derived from Egmont volcano (Fig. 1; Table 1). The tephras were correlated using a combination of stratigraphic position, field properties, ferromagnesian mineralogical assemblages (Lowe, 1988; Hodder et al., 1991; Newnham et al., 1995a), and new major element analyses of volcanic glass shards as reported below.

**Table 1 here*

Glass-shard major element compositions were obtained for nine samples from Kopuatai and eight samples from Moanatuatua (Tables 2 and 3, respectively) using a Jeol-JXA 'Superprobe' electron microprobe housed at the Analytical Facility, Victoria University of Wellington. The Kopuatai analyses were supplemented by previously-reported analyses on four cryptotephras and on Kaharoa Tephra (Table 2).

**Tables 2&3 here*

4.3.2 Radiocarbon dating

Fifty-five radiocarbon ages were obtained from the two sites (Fig. 2; Table 4). Of these, seven were radiometric dates on bulk peat samples, processed at the Waikato Radiocarbon Dating Laboratory, University of Waikato, Hamilton, New Zealand. These dated specific stratigraphic layers (base of sequence, tephra layers, and the clay layer in Kopuatai cores K106 and K204) and confirmed the preliminary field-based tephra identifications. Two of these bulk ages were taken from nearby cores not used in this study but are included here for completeness (Table 4).

**Table 4 here*

The remaining fourty-eight ages were determined by accelerator mass spectrometry (AMS) on above-ground plant macrofossils, processed at the NERC Radiocarbon Laboratory, East Kilbride, UK. These were spaced between the already well-dated Tuhua and Taupo tephra layers. Macrofossils used for dating were mainly *Leptospermum scoparium* and *Epacris pauciflora* leaves as these were generally common and well-preserved or, where these were absent or infrequent, *Epacris* and cf. *Empodisma* seeds, and *Gleichenia dicarpa* fronds.

4.3.3 Age-depth models

**Figure 3 here*

The age-depth models presented here (Fig. 3) were developed using the SHCal13 atmospheric curve (Hogg et al., 2013) in OxCal v4.3.2 (Bronk Ramsey, 2017). Both the 55 radiocarbon dates (Table 4) and preferred Lowe et al. (2013) ages for nine tephras (Table 1) were modelled using P_Sequence commands (Bronk Ramsey, 2008) for each of the six cores; outliers were analysed with the General model (Bronk Ramsey, 2009). Running the P_Sequence models together permits cross-referencing tephras between cores, treating these deposits as coeval isochrons.

5 Results

5.1. Kopuatai

The three Kopuatai cores comprise dark brown peat throughout, interbedded with millimetre-to-centimetre scale visible tephra layers. As noted earlier, two of the Kopuatai cores include a minerogenic layer dated to c. 7400−6900 cal yr BP and thereafter transitioning upwards into peat. As the light transmission properties of clay are distinctly different to those of peat, humification results are not presented for the clay layer and we restrict our comparisons of humification records to the period 6500—1700 cal yr BP, when peat formation is dominant at all six core sites.

In all three sequences, moisture content and TOC remain consistent at 90−95% and *c.* 60%, respectively, except around tephra layers. Marked oscillations are evident in the light transmission values which vary between 10−30% away from prominent tephra layers.

The light transmission curves for the three sequences are compared against a common timescale in Figure 4a. All three records show similar short-term oscillations superimposed on a long-term trend towards increasing light transmission (reduced humification) commencing between 5000 and 4000 cal yr BP.

**Figure 4 here*

In Figure 5a, the 100-year averages for the three detrended Kopuatai humification records are able to be compared. They display coherent intervals where all three records gave the same trend (positive or negative humification trends). Consistently wetter intervals are indicated for 3800–3300 cal yr BP and for 2000–1700 cal yr BP whereas the period 2400–2000 is mostly wetter than average. Consistently dry conditions are indicated for the interval 4900–4300 cal yr BP and the period 3300–2400 is mostly drier than average. Outside of these intervals, there is no coherent pattern indicated across the three records.

**Fig 5 here*

Correlation analysis indicates a significantly ($p<0.05$) positive relationship overall between the 100-year humification averages for K204 and the other two core records, but not between K106 and K108 (Table 5).

**Table 5 here*

5.3 Moanatuatua

The three Moanatutua cores, similar to the Kopuatai cores, comprise dark brown peat throughout, interbedded with millimetre-to-centimetre scale visible tephra layers as well as cryptotephra glass concentrations (Fig. SI2). In all three sequences, moisture content and TOC remain consistent at 85–90 % and *c*. 50 %, respectively, except around tephra layers. As for the Kopuatai cores, marked oscillations are evident in the light transmission values which range from 10–25 %.

The corrected light transmission curves for the three sequences are compared against a common timescale in Figure 4b. As at Kopuatai, there is a consistent long-term trend towards increasing light transmission values after *c*. 4500 cal yr BP.

Comparison of the three detrended Moanatuatua humification records in 100-year bins (Fig. 5b) shows mostly wetter intervals for 7000–6400 cal yr BP, 4600–4200 cal yr BP, 3600–3400 cal yr BP, 2900–2500 cal yr BP, and 2100–1700 cal yr BP. The intervals 5500–4600 cal yr BP and 4200– 3700 cal yr BP are mostly dry and 2500–2100 cal yr BP is consistently dry for all three records. Outside of these intervals, there is no coherent pattern indicated across the three records.

Correlation analysis indicates a significantly ($p<0.05$) positive relationship between the 100-year humification averages for M103 and M102 only with the other two core pairs not significantly correlated with one another (Table 5).

6 Discussion

6.1 Interpretation of peat humification records

Light transmission indicates the overall degree of peat humification for the estimated c. 20–40 year time period encapsulated by each sample. Large changes in humification should be predominantly representative of the average aeration at the bog surface during this interval, which in ombrotrophic bogs is a function of the balance between precipitation and evapotranspiration (P-E). Under normal conditions of a high and stable water table, seen today at Kopuatai and prior to drainage at Moanatuatua (Ratcliffe et al., 2019), bog surface wetness and hence P-E balance vary markedly through the seasonal cycle (Maggs, 1997; Fritz et al., 2008; Ratcliffe et al., 2019). During winter, the water table typically reaches a maximum and excess precipitation may be lost as runoff – during this time the water table rarely drops below a threshold that permits aerobic decay in the surface peat. The main period of peat decay is therefore the summer season when the near-surface peat is subject to biologically important changes in moisture and aeration and also to the highest temperatures. In Northern Hemisphere temperate peatlands, warm-season moisture deficit has been shown to be the main driver of decadal-scale changes in water table (Charman, 2007; Charman et al., 2009) and it seems likely that a similar relationship exists in New Zealand restiad peatlands. However, temperature can also be a direct driver of humification, independent of evaporation, through stimulation of microbial activity. In a number of bogs with very deep water tables, water table fluctuation can have little effect on peat surface moisture content, and thus decay, with humification almost entirely driven directly by temperature, rather than P-E and water table. This is the case in a number of un-modified bogs (Lafleur et al*.,* 2005*;* Euskirchen et al., 2014) and in Moanatuatua post-drainage (Ratcliffe et al., 2019). However, we would anticipate that any disconnect between water table and humification would be accompanied by a sustained shift towards high humification, itself indicative of a low frequency change in P-E. We are thus cautious about attributing high-frequency changes in humification to P-E in the more humified sections of the core but consider that the downcore variations in peat humification will generally reflect the combined effects of summer precipitation and temperature variability. 'Summer' in this context may actually be defined as an extended summer season covering all the months in moisture deficit rather than simply a notional December to February period (Charman et al., 2009).

6.2. Millennial-scale inferred moisture variability

The sampling strategy and analyses deployed here were designed to allow for the possibility of climate forcing of long-term (millennial scale) humification values by examining raw corrected light transmission values at this scale. As stated earlier, light transmission is inversely related to the degree of peat decomposition so the more decomposed or humified the sample, the less light transmitted. The underlying premise is that replicated patterns in humification between and within sites are more likely to represent regional climate signals.

The most striking pattern evident in all records at both sites is that corrected light transmission values show an increasing positive trend, indicating decreasing humification overall after c. 4000 cal yr BP, albeit with strong variability. Because the same long-term trends, well-constrained chronostratigraphically, are observed at these hydrologically-independent sites, a climate forcing should be considered, with a pervasive shift to a more positive P-E balance after c. 4000 cal yr BP being the most plausible conclusion. However, as discussed above, our approach does not preclude the possibility of long-term peat decay rather than climate determining any millennial scale trends and we point out that an increase in humification with age is what would be expected with progressive anaerobic decay over time. Therefore it is important to evaluate this postulated climate reconstruction against independent climate proxy records from these sites and also from the wider region.

6.3. Comparison with other New Zealand Holocene climate records

Holocene pollen records for Kopuatai (Newnham et al., 1995a) and Moanatuatua (Jara et al., 2017) have been interpreted as indicating a mid-Holocene change from comparatively warm, wet climate to drier, possibly frostier climate (Fig. 6). Key indicators for this change are the expansion of pollen of *Agathis australis,* which prefers dry conditions for growth, particularly in spring (Fowler & Boswijk, 2007), and the decline in the frost and drought sensitive *Ascarina lucida*. The *Agathis australis* pollen records at Kopuatai (Newnham et al., 1995a) and Moanatuatua (Jara et al., 2017) are insightful. *Agathis* was absent during the early Holocene, but expanded from c. 7000 - 5000 cal yr BP, a pattern evident in other records from the region (e.g. Newnham *et al*., 1989; 1991;1995a; 1995b; van den Bos *et al*., 2018). Dendroclimatological analyses of *Agathis australis* has shown the width of growth rings is strongly linked to ENSO, with wide rings associated with El Niño events (Fowler et al., 2007; 2012) when drier summers typically occur in the Waikato region.

These assertions are further supported by the pollen-climate reconstructions reported previously from Moanatuatua bog by Jara et al (2017). A pollen-derived moisture index independent of *Agathis* shows a long-term drying trend commencing by ca. 7000 cal. yr BP, although persistent below-average values are not observed until c. 3500 cal yr BP (Fig. 6). A similar drying trend is reported at Lake Pupuke, Auckland, ~90–130 km to the northwest of the study sites (van den Bos *et al*., 2018; Fig. 1; Fig. 6). At the same site, a Holocene summer temperature reconstruction derived using chironomids also provides informative insight into seasonal climate variability for the region (van den Bos et al., 2018). At Pupuke, reconstructed summer temperatures rise to peak in the mid-late Holocene, despite mean annual temperatures remaining comparatively constant, implying cooler winters (Fig. 6). Similar mean annual temperature patterns are reconstructed for Moanatuatua (Jara et al., 2017; Fig. 6). Taken together, these quantitative climate reconstructions from Auckland and Waikato are consistent with earlier observations for these regions during the late Holocene, and point strongly to comparatively warm, dry summers but cooler winters at that time. Similar conclusions were drawn from a multi-proxy study in southern South Island that incorporated pollen, testate amoebae, and humification analyses (Wilmshurst et al., 2002).

In contrast to these climate inferences drawn from the Kopuatai and Moanatuatua pollen records and from Pupuke chironomid and pollen records, a climate interpretation of our humification records from these sites would indicate primarily wetter summers during the interval *c*. 5000–2000 cal. yr BP, albeit punctuated at times by phases of dry summers (see below). We conclude therefore that this long-term trend signalling decreasing humification in younger sediments cannot be attributed to regional climate variability and is likely to be more indicative of long-term decay of peat.

6.4. Inferred moisture variability at decadal-centennial scales

Turning to the light transmission residuals (Fig. 5), we observe numerous decadal-centennial scale phases in all six records. As these residual values are assumed to be independent of any long-term decay effect, they seem likely to represent shorter-term variability in summer P-E balance along with other, local site factors. A less-thancomplete consistency across the records within and between sites suggests that local site factors at times may over-ride a regional climatic signal from an individual humification record. The most likely confounding factor arises from changes in vegetation composition at the core site over time, as has been pointed out for other regions (e.g. Chambers et al., 1997). Marked changes in vegetation composition over time at a particular core site have been reported previously from plant macrofossil analyses at Kopuatai (Newnham et al., 1995a) and Moanatuatua (Haenfling et al., 2015).

Other complicating factors could arise from specific characteristics of these restiad bog sites. The bog surfaces exhibit patterns of moist swales and intervening drier hummocks (Clarkson et al., 2004; McGlone, 2009) and it has been suggested that these features may migrate across the surface of the bog over time as part of a natural process of growth dynamics and hence independently of climate variability (McGlone, 2009). This process would likely cause variation in the degree of evapotranspiration and hence bog surface wetness experienced between hummocks and swales which would change as these topographic features migrated across the core sites. Also, the extensive Waikato restiad bogs may lack the climate sensitivity of smaller sites, which, together with the significant water holding properties of restionaceae rootlets (Clarkson et al., 2004), may serve to buffer the sites from paleohydrological change.

Nevertheless, there are some consistent patterns evident between the different humification records which points to broader scale climate processes that at times outweigh these local site factors. All six profiles show pronounced centennial-scale phases of predominantly wetter or drier summers suggesting that strong centennial scale variability in bog surface wetness was a prevalent feature of Holocene climate. Similar conclusions were drawn from the two previous New Zealand studies involving humification analyses, albeit from single peat profiles (McGlone & Wilmshurst, 1999; Wilmshurst et al., 2002). In the next section, we consider the climate forcing implications of these centennial scale shifts in Waikato bog surface wetness.

6.5. Climate forcing mechanisms

It is hardly surprising that Holocene climate proxy records from New Zealand display considerable spatio-temporal variability. Strong regional diversity is evident in the modern climate, arising from complex interactions between the main axial mountain ranges and the principal atmospheric circulation systems, played out across a broad latitudinal domain (e.g., Lorrey & Bostock, 2017). These distinctive spatial patterns are often accentuated by short-term climate variability, largely explained by the dynamic interplay between ENSO and SAM and their modulating effect on the Southern Westerly Winds (SWW) (Kidston et al., 2009; Ummenhofer and England, 2007). Largely for these reasons, previous explanations of New Zealand Holocene palaeoclimate variation have typically invoked changes in atmospheric circulation patterns operating on a hemispheric scale. Numerous records support the conclusion drawn by the Pole-Equator-Pole II (Asia-Australasian) group that the circum-Antarctic westerlies strengthened and possibly expanded equatorwards during the Late Holocene (Shulmeister *et al*., 2004; Lamy et al., 2010). Others have suggested intensification of ENSO from the mid-Holocene resulting in highly variable rainfall throughout New Zealand and the occurrence of severe droughts in eastern and southern regions (McGlone et al., 1992, McGlone and Wilmshurst, 1999). Given the interplay between ENSO/SAM and the SWW observed in modern climate today, all of these mechanisms may be relevant to the records presented here but, as precipitation variability today in the Waikato region of northern New Zealand is strongly linked to ENSO cycles (Ummenhofer and England, 2007), this is likely to be a dominant factor.

In the context of other proxy records from the region, the peat humification records at Moanatuatua and Kopuatai are consistent with the model of ENSO intensification. At these sites today, drier summers and droughts are more likely during El Niño phases, with increased precipitation from strengthened north-easterly rain-bearing winds during La Niña phases. A mid-Holocene transition towards drier summers, but with increasing variability and stronger seasonality including more extreme droughty summers, suggests that a strengthening of both phases of the ENSO cycle occurred. In pollen records, the late Holocene expansion of *Agathis australis* (described earlier) may also be linked to this ENSO strengthening as was first suggested by McGlone et al (1992). More recently, a quantitative precipitation record using carbon isotope ratios from leaves preserved in lake sediments from subtropical eastern Australia (27°S) revealed enhanced centennial-scale ENSO variability with more frequent El Niño event resulting in several dry anomalies after 3200 cal. yr BP (Barr et al., 2019).

Variation in strength of ENSO is thought to be due to precessional forcing affecting seasonal insolation values at low latitudes (Clement et al., 2001) although some paleoclimate data do not support this contention (Cobb et al., 2013). We suggest a similar driver for the enhanced seasonality evident in these Waikato bog-based records during the late Holocene. The difference between summer (December) and winter (June) insolation values for the approximate latitude of these sites increased progressively through the Holocene to a maximum at *c*. 2000 cal. yr BP. Increasing seasonality of local insolation would have exacerbated the precession-driven inter-annual variations and overall strengthening of ENSO at these sites, promoting frequency of summer drought despite an overall wetter climate over decadal scales. In contrast, during the Early Holocene, reduced seasonality coupled with weaker pole-to-equator temperature gradients are consistent with evidence for weaker ENSO forcing at that time (e.g. Rodbell et al., 1999; Moy et al., 2002).

At shorter timescales, the strong controls exerted by ENSO cycles on precipitation in the Waikato region today support the contention that they have contributed to the pronounced centennial-scale variability we observe in the humification residuals at both our bog sites. We test this assertion by comparing the Waikato bog humification records with the flagship Holocene record of ENSO events from Laguna Pallcacocha, Ecuador (Moy et al., 2002). For this comparison we have derived a regional humification record by summing the humification residuals for all six records in 100-year bins (Fig. 7). With this approach, we assume the regional climatic signal inherent across the six records is likely to overshadow any individual local site 'noise'. We test this assumption by comparing the composite regional record with a proxy index for water-table variability derived independently at a different core site at Moanatuatua Bog, using pollen corrosion analysis (Jara et al., 2017). This comparison (Fig. 7) shows a strong match between regional wet (dry) phases inferred from the composite humification record and phases of high (low) water table at Moanatuatua inferred from pollen corrosion.

Turning to the comparison with ENSO, at the centennial scale, the Laguna Pallcacocha record shows four phases of enhanced warm El Niño activity during the timeframe of our humification records (~6200–1700 cal yr BP) when the frequency of these events exceeded ten per century: at 5.7–5.5 cal yr BP, 5.0–4.8 cal yr BP, 3.0–2.8 cal yr BP, and 2.6–2.4 cal yr BP. Each of these four phases corresponds with relatively dry phases in northern New Zealand when composite light transmission residuals are approximately at or below average for the interval. Conversely, each of the five wettest Waikato phases inferred from the composite humification record, when summed light transmission residuals are ≥2, correspond to phases of reduced warm El Niño events (≤ 5 per century) when La Niña events can be assumed to be more frequent: at 6.2–6.0 cal yr BP, 4.4–4.2 cal yr BP, 3.5–3.4 cal yr BP, 2.8–2.6 cal yr BP, and 1.9–1.7 cal yr BP. We note that the last interval broadly corresponds with an inferred intense period of La Niña in concert with positive SAM reconstructed from a sedimentological record at Lake Tutira, east-central North Island (Gomez et al., 2012).

Although the teleconnection between these two records at distant points of the ENSO domain is not perfectly matched, the alignment of the more extreme phases of ENSO activity with Waikato paleohydrology demonstrates the potential of peat humification analyses of Waikato bogs to serve as a proxy for paleo ENSO. Similar assertions have been drawn using peat humification records from northeast Queensland (Turney et al., 2004, Burrows et al., 2014)

7.0. Conclusions

There is considerable interest in developing longer-term reconstructions of SWW shifts and associated key modes of climate variability such as SAM and ENSO. However, as recently pointed out by Turney et al. (2017), there is much regional variability in these climate modes whilst the timing of maximum westerly airflow strength and its core latitude may also vary considerably in time and space. Not surprisingly, these complexities raise questions over the value of extending reconstructions from one region to the wider hemisphere (Fletcher and Moreno, 2012). On the other hand, if the local climate signatures for the different phases of these climate modes are well understood, and if they can be translated with confidence into local climate proxies that can be shown to vary consistently across multiple well-dated sedimentary records, then regional-hemispheric comparisons are a viable and potentially powerful means of reconstructing these past modes of climate variability.

The underlying premise to the current study is that a conceptual relationship between peat humification analysis and paleohydrology potentially has an important contribution to this effort. The primary rationale has been to assemble multiple records of peat humification to test their suitability as a proxy for past effective precipitation in northern New Zealand, where precipitation variability is a key manifestation of ENSO cycles. We sought to mitigate some of the confounding factors reported previously for humification analysis by developing robust independent chronologies for each of the six records, based on high resolution, local, ^{14}C dating, and an independently-derived tephrochronological record, and by targeting two hydrologically separate but ecologically similar raised bogs from the Waikato region. We applied an underpinning rationale that replicability across these records would point strongly to climatic forcing of humification trends over and above other confounding factors.

Our results suggest that humification records from ombrogenous bogs can provide insight into past climate dynamics but that non-climatic confounding factors must also be critically considered. We argue from comparison with independent climate proxy records that slow anaerobic decomposition of the peat deposits over time rather than climate best explains a long-term trend in humification, despite this trend being observed in all six records. On the other hand, once this decay factor is detrended, replication between records provides a useful approach, both in terms of testing the applicability of the method in a certain region or site, and in developing a level of confidence in any paleoclimate assertions drawn. An important ramification from this study is that a single humification record may not always be reliable for indicating wet-dry shifts at decadal-centennial timescales, as has also been found at other multi-site humification studies (Payne & Blackford, 2008; Amesbury et al., 2012). The most likely confounding local site factors are changing vegetation at the core site over time affecting the composition and decomposition of accumulating peat, which occurred at both sites. Another factor at these sites may be changes in local topography over time.

Despite these likely local confounding factors, when our six humification records are aggregated at the regional level, they display good correspondence with key phases of the well-documented Holocene ENSO record at Laguna Pallcacocha in the eastern Equatorial Pacific. Within the timeframe common to the two records the most prominent phases of El Niño at Pallcacocha coincide with relatively dry intervals at Waikato, consistent with local signatures of El Niño climate. Conversely, all of the wettest phases in the Waikato record coincide with inferred extensive La Niña phases at Pallcacocha, again consistent with local Waikato signatures of ENSO climate variability. Among the latter, the interval 2.1–1.7 cal ka stands out as a pronounced wet phase in all six humification records, in line with findings from previous work in eastern North Island that invokes sustained La Niña and positive SAM conditions at this time. Other less-pronounced centennial-scale shifts in bog surface wetness are a pervasive feature of all six records with varying degrees of overlap in time, and may arise from other permutations of these predominant climate forcing mechanisms. Future work aimed at showing how these modes of climate variability have operated in the past could be informed by replicated humification records from New Zealand's raised bogs.

Acknowledgements

We thank the Department of Conservation (Hamilton) and Wallace Farm for coring permission and access, and a number of colleagues for valued assistance with field work and laboratory analyses at Plymouth and Waikato universities, in particular Phil Hodges, Annette Rodgers, and other technical staff of the School of Science at University of Waikato. Dr Ganqing Xu (University of Waikato) helped Lowe prepare samples for electron microprobe analyses, which were undertaken by Dr Kathryn Wilson with support from John Patterson (Victoria University of Wellington). Drs Fiona Petchey and Alan Hogg (Waikato Radiocarbon Dating Laboratory) are thanked for assistance with the Waikato dates and Joss Ratcliffe (University of Waikato) for helpful discussion on interpretation of humification records. The AMS radiocarbon dates were funded by the NERC Radiocarbon Facility (Environment) Allocation 948.1201. This work was supported by a research grant from the Leverhulme Trust (Grant Ref: RPG-2015-394). The paper is an output also of the EXTRAS project "EXTending TephRAS as a global geoscientific research tool stratigraphically, spatially, analytically, and temporally" led by the International focus group on tephrochronology and volcanism (INTAV) of the Stratigraphy and Chronology Commission (SACCOM) of the International Union for Quaternary Research (INQUA) for 2015-2019. Finally, we are grateful to two referees who provided very useful comments and references that enabled us to improve the paper.

References

Aaby B, Tauber H. 1975 Rates of peat formation in relation to degree of humification and local environment, as shown by studies of a raised bog in Denmark. *Boreas* **4:** 1-17

Abram N, Mulvaney R, Vimeux F, Phipps SJ, Turner J, England MH, 2014. Evolution of the Southern Annular Mode during the past millennium. *Nat. Clim. Change* **4**: 564–569.

Alloway BV, Westgate JA, Pillans B, Pearce N, Newnham RM, Byrami M, Aarburg S. 2004. Stratigraphy, age and correlation of middle Pleistocene silicic tephras in the Auckland region, New Zealand: a prolific distal record of TVZ volcanism. *New Zealand Journal of Geology & Geophysics* **47**: 447-479

Amesbury MJ, Barber KE, Hughes PDM. 2012. The relationship of fine-resolution, multi-proxy palaeoclimate records to meteorological data at Fågelmossen, Värmland, Sweden and the implications for the debate on climate drivers of the peat-based record. *Quaternary International* **268**: 77-86

Amesbury M, Charman DJ, Newnham RM, Loader NJ, Goodrich JP, Royles J, Campbell DI, Keller DE, Baisden T, Roland TP, Gallego-Sala AV, 2015. Can oxygen stable isotopes be used to track precipitation moisture source in vascular plant dominated peatlands? *Earth and Planetary Science Letters* **430**: 149-159.

Amesbury M, Charman DJ, Newnham RM, Loader NJ, Goodrich JP, Royles J, Campbell DI, Roland TP, Gallego-Sala AV, 2015. Carbon stable isotopes as a palaeoclimate proxy in vascular plant dominated peatlands. *Geochimica et Cosmochimica Acta*, 164, 161-174

Ballinger, M.J. 2003. Developing methods for identifying cryptic tephra in peat cores from the Waikato region, North Island, New Zealand. MRes thesis, University of Plymouth, Plymouth, UK.

Barber KE. 1981. *Peat stratigraphy and climatic change: a palaeoecological test of the theory of cyclic peat bog regeneration*. Balkema, Rotterdam.

Barr C, Tibby J, Leng M, Tyler J, Henderson A, Overpeck J, Simpson G, Cole J, Phipps S, Marshall J. 2019. Holocene El Niño–southern Oscillation variability reflected in subtropical Australian precipitation. *Scientific reports* 9: 1627, 2019.

Blackford JJ, Chambers FM. 1993. Determining the degree of peat decomposition for peat-based palaeoclimate studies. *International Peat Journal* **5**: 7-24.

Borgmark A, Wastegård S. 2008. Regional and local patterns of peat humification in three raised peat bogs in Värmland, south-central Sweden. *GFF* **130**: 161-176.

Bronk Ramsey C. 2008. Deposition models for chronological records. *Quaternary Science Reviews* **27(1-2)**: 42-60.

Bronk Ramsey C. 2009. Dealing with outliers and offsets in radiocarbon dating. *Radiocarbon* **51(3)**: 1023-1045.

Campbell DI, Williamson JL. 1997. Evaporation from a raised bog. *Journal of Hydrology* **193**: 142-160.

Campbell DI, Jackson R. 2004. Hydrology of wetlands. In Harding, J.S., Mosley, P., Pearson, C. and Sorrell, B.K., editors, *Freshwaters of New Zealand, New Zealand Hydrological Society and New Zealand Limnological Society, Christchurch*, 20.1-20.14.

Caseldine C, Baker A, Charman D, Hendon D. 2000. A comparative study of optical properties of NaOH extracts: implications for humification studies. *The Holocene* **10:** 649-658.

Chambers FM, Barber KE, Maddy D, Brew J. 1997. A 5500-year proxy-climate and vegetational record from blanket mire at Talla Moss, Peebleshire, Scotland. *The Holocene* **7**: 391-399.

Chambers FM, Beilman DW, Yu Z. 2011. Methods for determining peat humification and for quantifying peat bulk density, organic matter and carbon content for palaeostudies of climate and peatland carbon dynamics. *Mires and Peat* **7 (7)**: 1-10.

Chambers FM, Booth RK, De Vleeschouwer F, Lamentowicz M, Le Roux G, Mauquoy D, Nichols JE, van Geel B. 2012. Development and refinement of proxy-climate indicators from peats. *Quaternary International* **268**: 21–33.

Charman DJ. 2007. Summer water deficit controls on peatland water table changes: implications for Holocene palaeoclimate reconstructions. *The Holocene* **17**: 217-227.

Clarkson BR. 2002. Swamps, fens and bogs. In Clarkson BD, Merrett M. and Downes T, editors, *Botany of the Waikato*, Waikato Botanical Society, Hamilton, 49-58.

Clarkson BR, Thompson K, Schipper LA, McLeod M, 1999. Moanatuatua Bog – proposed restoration of a New Zealand restiad peat bog ecosystem. In Streever W, editor, *An international perspective on peatland rehabilitation*, Kluwer, The Netherlands, 127-137.

Clarkson BR, Schipper LA, Lehmann A. 2004. Vegetation and peat characteristics in the development of lowland and restiad peat bogs, North Island, New Zealand. *Wetlands* **24**: 133-151.

Clement A, Cane M, Seager R. 2001. An orbitally driven tropical source for abrupt climate change. *Journal of Climatology* **14**: 2369-2375.

Cobb KM, Westphal N, Sayani HR, Watson JT, Di Lorenzo E, Cheng H, Edwards R. L, Charles CD. 2013. Highly Variable El Niño-Southern Oscillation throughout the Holocene. *Science* **339**: 67–70.

Cranwell LM. 1939. Native vegetation. Soils and agriculture of part of Waipa County. Dept. of Scientific and Industrial Research, Wellington, pp. 23–29 https://doi.org/10.7931/DL1-SBP-0005

Cranwell LM, von Post L. 1936. Post-Pleistocene Pollen Diagrams from the Southern Hemisphere. *Geografiska Annaler* **18**:3-4, 308-347, DOI: 10.1080/20014422.1936.11880619

Clymo RS1984. The limits to peat bog growth. *Philosophical Transactions of the Royal Society of London B* **303**, 605-654

Damaschke, M., Cronin, S.J., Holt, K.A., Bebbington, M.S., Hogg, A.G., 2017. A 30,000 yr high-precision eruption history for the andesitic Mt Taranaki, North Island, New Zealand. *Quaternary Research* **87**, 1-23.

Davoren A. 1978. A survey of New Zealand peat resources. *Water and Soil Technical Publication No. 14,* 155 pp.

de Lange P, Heenan P, Clarkson BD, Clarkson BR. 1999. Taxonomy, ecology, and conservation of Sporadanthus (Restionaceae) in New Zealand. *New Zealand Journal of Botany* **37**: 413-431.

de Lange PJ, Lowe DJ, 1990. History of vertical displacement of Kerepehi Fault at Kopuatai bog, Hauraki Lowlands, New Zealand, since c. 10,700 years ago. *New Zealand Journal of Geology and Geophysics* **33**: 277-283.

Edbrooke SW. (compiler) 2001. *Geology of the Auckland area:* Institute of Geological and Nuclear Sciences 1:250,000 Geological Map 3. 1 sheet and 74 pp. IGNS, Lower Hutt.

Edbrooke SW. (compiler) 2005. *Geology of the Waikato area*. Institute of Geological and Nuclear Sciences 1:250,000 Geological Map 4. 1 sheet and 68 pp. IGNS, Lower Hutt.

Elliot M, Neall V, Wallace C. 2005. A late Quaternary pollen record from Lake Tangonge, far northern New Zealand. *Reviews of Palaeobotany and Palynology* **136**: 143-158.

Euskirchen ES, Edgar CW, Turetsky MR, Waldrop MP, Harden JW. 2014. Differential response of carbon fluxes to climate in three peatland ecosystems that vary in the presence and stability of permafrost. *J. Geophys. Res. Biogeosciences* 119: 1576–1595. https://doi.org/10.1002/2014JG002683

Fogt RL, Perlwitz J, Monaghan AJ, Bromwich DH, Jones JM, Marshall GJ. 2009. Historical SAM variability. Part II: Twentieth-century variability and trends from reconstructions, observations and the IPCC AR4 models. *J. Clim*. **22**: 5346-5365

Fowler A, Boswijk G. 2007. Five centuries of ENSO history recorded in Agathis Australis (kauri) tree rings. *PAGES News* **15(2)**: 20-21.

Fowler A, Boswijk G, Gergis J, Lorrey A. 2007. ENSO history recorded in Agathis australis (kauri) tree rings. Part A: kauri's potential as an ENSO proxy. International *Journal of Climatology 28*: 21 – 35.

Fowler A, Boswijk G, Lorrey A, Gergis J, Pirie M, McCloskey SPJ, Wunder J, 2012. Multi-centennial tree-ring record of ENSO-related activity in New Zealand. *Nature Climate Change* ***2***: 172-176.

Fritz C, Campbell DI, Schipper LA. 2008. Oscillating peat surface levels in a restiad wetland, New Zealand – magnitude and spatiotemporal variability. *Hydrological Processes* **22**: 3264-3274.

Froggatt PC. 1983. Toward a comprehensive Upper Quaternary tephra and ignimbrite stratigraphy in New Zealand using electron microprobe analysis of glass shards. *Quat. Res*. **19**: 188-200.

Garreaud RD, 2007. Precipitation and circulation covariability in the extratropics, *J. Clim*. **20(18)**: 4789–4797.

Gehrels MJ, Lowe DJ, Hazell ZJ, Newnham RM. 2006. A continuous 5300-year Holocene cryptotephrostratigraphic record from northern New Zealand and implications for tephrochronology and volcanic-hazard assessment. *The Holocene* **16:** 173-187.

Gehrels, M.J., Newnham, R.M., Lowe, D.J., Wynne, S., Hazell, Z.J., Caseldine, C. 2008. Towards rapid assay of cryptotephra in peat cores: Review and evaluation of selected methods. *Quaternary International* 178, 68-84.

Gomez B, Carter L, Orpin AR, Cobb K, Page MJ, Trustrum N, Palmer A. 2012. ENSO/SAM interactions during the middle and late Holocene. *The Holocene* **22**: 23–30.

Goodrich, J. P., Campbell, D. I., Roulet, N. T., Clearwater, M. J., & Schipper, L. A. 2015. Overriding control of methane flux temporal variability by water table dynamics in a Southern Hemisphere, raised bog. *Journal of Geophysical Research: Biogeosciences* **120(5)**: 819-831. doi:10.1002/2014JG002844

Goodrich JP, Campbell DI, Schipper LA. 2017. Southern Hemisphere bog persists as a strong carbon sink during droughts. *Biogeosciences* **14**: 4563-4576.

Haenfling C, Newnham RM, Rees A, Jara I, Homes A, Clarkson B. 2017. Holocene history of a raised bog, northern New Zealand, based on plant cuticles. *The Holocene* **27**: 309-314.

Hartmann, DL, et al. 2013. Observations: Atmosphere and Surface. In Stocker, T. et al. (eds.) *Climate Change 2013: The Physical Science Basis.* Cambridge: CUP, 159-254.

Hazell Z, 2004. Holocene palaeoclimate reconstruction from New Zealand peatlands. Unpublished Ph.D. thesis, University of Plymouth, UK.

Hodder APW, de Lange PJ, Lowe DJ. 1991. Dissolution and depletion of ferromagnesian minerals from Holocene tephras in an acid bog, New Zealand, and implications for tephra correlation. *Journal of Quaternary Science* **6**: 195-208.

Hogg AG, Higham TFG, Lowe DJ, Palmer J, Reimer P, Newnham RM. 2003. A wiggle-match date for Polynesian settlement of New Zealand. *Antiquity* **77**: 116-125.

Hogg AG, Lowe DJ, Palmer JG, Boswijk G, Bronk Ramsey C, 2012. Revised calendar date for the Taupo eruption derived by 14C wiggle-matching using a New Zealand kauri 14C calibration data set. *The Holocene* **22**: 439-449. 10.1177/0959683611425551.

Hogg, A.G., Hua, Q., Blackwell, P.G., Niu, M., Buck, C.E., Guilderson, T.P., Heaton, T.J., Palmer, J.G., Reimer, P.J., Reimer, R.W., Turney, C.S.M., & Zimmerman, S. R.H. 2013. SHCal13 Southern Hemisphere Calibration, 0-50,000 Years cal BP. *Radiocarbon* **55(4)**: 1889–1903.

Hughes PDM, Mallon G, Essex HJ, Amesbury MJ, Charman DJ, Blundell A, Chambers FM, Daley TJ, Mauquoy D. 2012. The use of k-values to examine plant ‘species signals’ in a peat humification record from Newfoundland. *Quaternary International* **268**:156-165

Jara, I.A., Newnham, R.M., Alloway, B.V., Wilmshurst, J.M., Rees, A.B.H., 2017. Pollen-based temperature and precipitation records of the past 14,600 years in northern New Zealand (37°S) and their linkages with the Southern Hemisphere atmospheric circulation. *The Holocene* **27(1)**: 1756-1768. DOI: 10.1177/0959683617708444

Jarosewich, E., 2002. Smithsonian microbeam standards. *Journal of Research of the National Institute of Standards and Technology* **107**: 681-685.

Jarosewich, E., Nelen, J.A., Norberg, J.A., 1980. Reference samples for electron microprobe analysis. *Geostandards Newsletter* **4**: 43-47.

Jones JM, Gille ST, Goosse H, et al., 2016. Assessing recent trends in high-latitude Southern Hemisphere surface climate. *Nature Climate Change* **6**: 917-926. doi: 10.1038/nclimate3103

Kidston, J., Renwick, J. A., McGregor, J., 2009. Hemispheric-scale seasonality of the Southern Annular Mode and impacts on the climate of New Zealand. J. Climate, 22, 4759–4770.

Kottek M, Grieser J, Beck C, Rudolf B, Rubel F. 2006. World map of the Köppen-Geiger climate classification updated. *Meteorologische Zeitschrift* 15, 259-263.

Kuder, T., Kruge, M., Shearer, J., Miller, S. 1998. Environmental and botanical controls on peatification – a comparative study of two New Zealand restiad bogs using Py-Gc/Ms, petrography and fungal analysis. International Journal of Coal Geology 37, 3-27.

Lafleur PM, Moore TR, Roulet NT, Frolking S. 2005. Ecosystem respiration in a cool temperate bog depends on peat temperature but not water table. *Ecosystems*: 8, 619–629. https://doi.org/10.1007/s10021-003-0131-2

Lamy F, Kilian R, Arz HW, Francois JP, Kaiser J, Prange M, Steinke T. 2010. Holocene changes in the position and intensity of the southern westerly wind belt. *Nature Geoscience* **3(10)**, 695-699.

Langdon, PG, Hughes, PDM, Brown AG. 2012 Peat stratigraphy and climate change. *Quaternary International* **268**:1-8.

Lorrey AM, Vandergoes MJ, Almond PC, Renwick JR, Stephens T, Bostock H, Mackintosh A, Newnham RM**,** Williams PW, Ackerley D, Neil H, Fowler AM. 2012. Palaeocirculation across New Zealand during the last glacial maximum at ~21 ka. Quat Sci Rev 36:189-213.

Lorrey, A.M., Bostock, H. 2017. The climate of New Zealand through the Quaternary. In: Shulmeister, J. (ed.), Landscape and Quaternary Environmental Change in New Zealand, Atlantis Advances in Quaternary Science 3, 67-139. DOI 10.2991/978-94-6239-237-3_367

Lowe DJ, 1988. Stratigraphy, age, composition, and correlation of late Quaternary tephras interbedded with organic sediments in Waikato lakes, North Island, New Zealand. *NZ. J. Geol. Geophys.* **31**: 125-165.

Lowe DJ. 2011. Tephrochronology and its application: a review. *Quaternary Geochronology* **6**: 107-153.

Lowe DJ, Newnham RM, Ward CM. 1999: Stratigraphy and chronology of a 15 ka sequence of multi-sourced silicic tephras in a montane peat bog, eastern North Island, New Zealand. *New Zealand Journal of Geology and Geophysics* **42**: 565-579.

Lowe DJ, Shane PAR, Alloway BV, Newnham RM. 2008: Fingerprints and age models for widespread New Zealand tephra marker beds erupted since 30,000 years ago: a framework for NZ-INTIMATE. *Quaternary Science Reviews* **27**: 95-126.

Lowe, D.J., Blaauw, M., Hogg, A.G., Newnham, R.M. 2013. Ages of 24 widespread tephras erupted since 30,000 years ago in New Zealand, with re-evaluation of the timing and palaeoclimatic implications of the late-glacial cool episode recorded at Kaipo bog. *Quaternary Science Reviews* **74**: 170-194.

Lowe, D.J., Pearce, N.J.G., Jorgensen, M.A., Kuehn, S.C., Tryon, C.A., Hayward, C.L. 2017. Correlating tephras and cryptotephras using glass compositional analyses and numerical and statistical methods: review and evaluation. *Quaternary Science Reviews* **175**: 1-44.

Maggs G. 1997. Hydrology of the Kopuatai peat dome. *New Zealand Journal of Hydrology* **36**: 147-172.

Manville, V., Wilson, C.J.N. 2004. The 26.5 ka Oruanui eruption, New Zealand: a review of the roles of volcanism and climate in the post-eruptive sedimentary response. *N.Z. Journal of Geology and Geophysics* **47**: 525-547

Marshall GJ. 2003. Trends in the southern annular mode from observations and reanalyses. *J. Climate* **16**, 4134-4143.

McCormac F, Hogg A, Blackwell P, Buck C, Higham T, Reimer P. 2004. SHCal04 Southern Hemisphere calibration, 0-11.0 cal. kyr BP. *Radiocarbon* **46**: 1087-1092.

McGlone MS. 1988: New Zealand. In Huntley B, Webb T, editors, *Vegetation history: handbook of vegetation science Volume 7*. Kluwer Academic Publishers, 557-599.

McGlone MS. 2009. Postglacial history of New Zealand wetlands and implications for their conservation. *New Zealand Journal of Ecology* **33**: 1-23.

McGlone MS, Kershaw AP, Markgraf, V. 1992. El Niño/Southern Oscillation climatic variability in Australasian and South American paleoenvironmental records. In Diaz H, Markgraf V, editors, *El Niño: historical and paleoclimatic aspects of the Southern Oscillation*. University of Arizona Press, 435-462.

McGlone MS, Moar NT, 1977. The Ascarina decline and post-glacial climatic change in New Zealand. *New Zealand Journal of Botany* **15**, 485-489.

McGlone MS, Turney CSM, Wilmshurst JM. 2004. Late-glacial and Holocene vegetation and climatic history of the Cass basin, central south island, New Zealand. *Quaternary Res.* **62**: 267–279. doi: 10.1016/j.yqres.2004. 09.003

McGlone MS, Wilmshurst JM. 1999. A Holocene record of climate, vegetation change and peat bog development, east Otago, South Island, New Zealand. *Journal of Quaternary Science* 14(3): 239-254.

McGlone MS, Richardson SJ, Burge OR, Perry GLW, Wilmshurst JM. 2017. Palynology and the Ecology of the New Zealand Conifers. *Front. Earth Sci.* **5**:94. doi: 10.3389/feart.2017.00094

Morgan TJ, Herod AA, Brain SA, Chambers FM, Kandiyoti R. 2005. Examination of soil contaminated by coal-liquids by size-exclusion chromatography in 1-methyl-2-pyrrolidinone solution to evaluate interference from humic and fulvic acids and extracta from peat *Journal of Chromatography* **1095**: 81-88.

Moy CM, Seltzer GO, Rodbell DT, Anderson DM. 2002. Variability of El Niño/Southern Oscillation activity at millennial timescales during the Holocene epoch. *Nature* **420(6912)**: 162–165

Newnham RM, Lowe DJ, Green JD. 1989. Palynology, vegetation and climate of the Waikato lowlands, North Island, since c. 18,000 years ago. *Journal of the Royal Society of New Zealand* **19**: 127-150.

Newnham RM, Lowe DJ. 1991. Holocene vegetation and volcanic activity, Auckland Isthmus, New Zealand. *Journal of Quaternary Science* **6**: 177-193.

Newnham RM, Ogden J, Mildenhall DC, 1993.Late Pleistocene vegetation history of the Far North of New Zealand. *Quaternary Research* **39:** 361-372.

Newnham RM, de Lange P, Lowe DJ. 1995a. Holocene vegetation, climate and history of a raised bog complex, northern New Zealand based on palynology, plant macrofossils and tephrochronology. *The Holocene* **5(3)**: 267-282.

Newnham RM, Lowe DJ, Wigley GNA. 1995b. Late Holocene palynology and palaeovegetation of tephra-bearing mires at Papamoa and Waihi Beach, western Bay of Plenty, North Island, New Zealand. *Journal of Royal Society of New Zealand* **25**: 283-300

Newnham RM, Lowe DJ, McGlone MS, Wilmshurst JM, Higham T. 1998: The Kaharoa Tephra as a critical datum for earliest human impact in northern New Zealand. *Journal of Archaeological Science* **25**: 533-544.

Newnham RM, Lowe DJ, Alloway BV. 1999. Volcanic hazards in Auckland New Zealand: a preliminary assessment of the threat posed by central North Island silicic volcanism based on the Quaternary tephrostratigraphical record. In Firth C, McGuire WJ (eds) *Volcanoes in the Quaternary,* Geological Society, London, Special Publications **161**: 27-45.

Newnham RM, Vandergoes MJ, Sykes E, Carter L, Wilmshurst JM, Lowe, D.J., McGlone MS, Sandiford A. 2012. Does the bipolar seesaw extend to the southern mid-latitudes? *Quaternary Science Reviews* **36**: 214-222

NIWA 2009. Climate summaries for 1971-2000 period (Hamilton). CliFlo National Institute of Water and Atmospheric Research National Climate Database on the Web. http://CliFlo.niwa.co.nz/. Retrieved 19 Feb, 2009.

Ogden J, Newnham RM, Palmer JG, Serra R, Mitchell ND, 1993. Climatic implications of macro-and micro-fossil assemblages from late Pleistocene deposits in northern New Zealand. *Quaternary Research* **39:** 107-119

Payne RJ, Blackford JJ. 2009. Peat humification and climate change: a multi-site comparison from mires in south-east Alaska. *Mires and Peat* **3:** Art. 9. (Online: http://www.mires-and-peat.net/pages/volumes/map03/map0309.php)

Persaud M, Villamor P, Berryman KR, Ries W, Cousins WJ, Litchfield N, Alloway BV. 2016. The Kerepehi Fault, Hauraki Rift, North Island, New Zealand: active fault characterisation and hazard. *New Zealand Journal of Geology and Geophysics* **59**: 117-135.

Pronger, J., Schipper, L.A., Hill, R.B., Campbell, D.I., McLeod, M. 2014. Subsidence rates of drained agricultural peatlands in New Zealand and the relationship with time since drainage. *Journal of Environmental Quality* **43**: 1442-1449.

Ratcliffe JL, Campbell DI, Clarkson BR, Wall AM, Schipper LA. 2019. Water table fluctuations control CO_2 exchange in wet and dry bogs through different mechanisms. *Science of the Total Environment* **655**: 1037-1046. https://doi.org/10.1016/j.scitotenv.2018.11.151

R Core Team, 2016. R: A language and environment for statistical computing. R Foundation for Statistical Computing, Vienna, Austria. URL https://www.R-project.org/.

Renwick JA. 2005. Persistent positive anomalies in the Southern Hemisphere circulation. *Monthly Weather Review* **133(4)**: 977–988.

Rodbell DT, Seltzer G.O., Anderson DM, Abbott MB, Enfield DB, Newman JH. 1999. An 15,000-year record of El Niňo-driven alluviation in southwestern Ecuador. *Science* **283**: 516– 520.

Roos-Barraclough F, van der Knaap W, van Leeuwen J, Shotyk W. 2004. A late-glacial and Holocene record of climatic change from a Swiss peat humification profile. *The Holocene* **14**: 7–19.

Salinger MJ; Mullan AB. 1999. New Zealand climate: Temperature and precipitation variations and their links with atmospheric circulation 1930-1994. *International Journal of Climatology* **19**:1049-1071.

Schipper LA, McLeod M. 2002. Subsidence rates and carbon losses in peat soils following conversion to pasture in the Waikato region, New Zealand. *Soil Use and Management* **18**: 91-93.

Selby MJ, Lowe DJ. 1992. The middle Waikato Basin and hills. In Soons JM, Selby MJ, editors, *Landforms of New Zealand*. Second Edition. Auckland, Longman Paul, 233-255.

Shearer J. 1997. Natural and anthropogenic influences on peat development in Waikato/Hauraki Plains restiad bogs. *Journal of the Royal Society of New Zealand* **27**: 295-313.

Shulmeister J, Goodwin I, Renwick J, Harle K, Armand L, McGlone MS, Cook E, Dodson J, Hesse PP, Mayewski P, Curran M. 2004. The Southern Hemisphere westerlies in the Australasian sector over the last glacial cycle: a synthesis. *Quaternary International* **118-119**: 23-53.

Sparks RJ, Melhuish WH, McKee JWA, Ogden J, Palmer JG. 1995. ^{14}C calibration in the Southern Hemisphere and the date of the last Taupo eruption: evidence from tree-ring sequences. *Radiocarbon* **37**: 155-163.

Sparks RJ, Graham IJ, Morgenstern U. 2008. Cosmic chronometers. In Graham, I.J., chief editor, A continent on the move: New Zealand geoscience into the 21st century, *Geological Society of New Zealand, Miscellaneous Publication* **124**: 64-67. Lower Hutt.

Telford R, Heegaard E, Birks H. 2004a. All age-depth models are wrong: but how badly? *Quaternary Science Reviews* **23**: 1-5.

Telford R, Heegaard E, Birks H. 2004b. The intercept is a poor estimate of a calibrated radiocarbon age. *The Holocene* **14**: 296-298.

Thompson M, Campbell D, Spronken-Smith R. 1999. Evaporation from natural and modified raised peat bogs in New Zealand. *Agricultural and Forest Meteorology* **95**: 85-98.

Thompson DW, Solomon JS, Kushner PJ, England MH, Grise KM, Karoly DJ. 2011. Signatures of the Antarctic ozone hole in Southern Hemisphere surface climate change. *Nature Geoscience* **4**: 741-749.

Turney CSM, Wilmshurst JM, Jones RT, Wood JR, Palmer JG, Hogg AG, Thomas Z. 2017. Reconstructing atmospheric circulation over southern New Zealand: Establishment of modern westerly airflow 5500 years ago and implications for Southern Hemisphere Holocene climate change. *Quaternary Science Reviews* **159**: 77-87.

Ummenhofer CC**,** England MH. 2007. Interannual extremes in New Zealand precipitation linked to modes of Southern Hemisphere climate variability. *Journal of Climate* **20**: 5418-5440

van den Bos V, Rees ABH, Newnham RM, Vandergoes MJ, Wilmshurst JM, Augustinus PC. 2018. Holocene temperature, humidity and seasonality in northern New Zealand linked to Southern Hemisphere summer insolation. *Quaternary Science Reviews* **201**: 77-88

Wagstaff SJ, Clarkson BR. 2012. Systematics and ecology of the Australasian genus Empodisma (Restionaceae) and description of a new species from peatlands in northern New Zealand. *PhytoKeys* **13**: 39-79.

Wang C, Cai W. 2013. Climate-change impact on the 20th-century relationship between the Southern Annular Mode and global mean temperature. *Nat. Sci. Rep*. 3: DOI:10.1038/srep02039.

Williams PW, King DNT, Zhao J-X, Collerson KD. 2004. Speleothem master chronologies: combined Holocene ^{18}O and ^{13}C records from the North Island of New Zealand and their palaeoenvironmental interpretation. *The Holocene* **14**: 194-208.

Wilmshurst, J.M., McGlone, M.S. 1996. Forest disturbance in the central North Island, New Zealand, following the 1850 BP Taupo eruption. The Holocene 6, 399-411.

Wilmshurst JM, McGlone MS, Charman DJ. 2002. Holocene vegetation and climate change in southern New Zealand: linkages between forest composition and quantitative surface moisture reconstructions from an ombrogenous bog. *Journal of Quaternary Science* **17**: 653-666.

Yeloff D, Mauquoy D. 2006. The influence of vegetation composition on peat humification: implications for palaeoclimatic studies. *Boreas* **35**: 662-673.

Figure Captions

Figure 1. *a*) Regional setting of New Zealand in southwest Pacific Ocean, showing principle atmospheric circulation systems and ocean currents; **b**) part of North Island with site locations; **c)** and **d)** locations of coring sites at Kopuatai bog and Moanatuatua bog, respectively. Elevations (triangles) are in metres above sea level.

Figure 2. Stratigraphy of peat cores at Kopuatai and Moanatuatua showing positions of tephras and cryptotephras in them (ages are given in Table 1) along with ^{14}C sampling positions (laboratory codes and other details are given in Table 4).
[a]Stratigraphy after Gehrels et al. (2006)
[b]Grid reference of the New Zealand Topo50 series (1: 50,000)
[c]Identification after Ballinger (2003)
[d]Identification after Gehrels et al. (2008); other identifications after Hazell (2004)
[e]These two ^{14}C samples were taken from an immediately adjacent core (at BE34 090001) (Hazell, 2004)

Figure 3. Linearly-interpolated age-depth models for Kopuatai (a) and Moanatuatua (b). Tephra ages are indicated by tephra names, and AMS radiocarbon ages by lab code. Error bars indicate radiocarbon calibration errors (2-sigma ranges).

Figure 4. Corrected light transmission plotted against age for (a) the three Kopuatai cores and (b) the three Moanatuatua cores. Bolder curves indicate three-point running mean.

Figure 5. Light transmission residuals averaged in 100-year bins for a) three Kopuatai cores, 6200–1700 cal yr BP and b) three Moanatuatua cores, 7000–1700 cal yr BP. Each bar consists of 3 segments, each representing the average light transmission value for that period at one core site.

Figure 6. Comparison of Holocene climate proxy records from Waikato and Auckland for the interval 16,000 yr BP to present. From top to bottom, period of *Agathis australis* expansion at Kopuatai Bog (Newnham et al., 1995a); composite light transmission records for Kopuatai and Moanatuatua bogs (data, this study, Fig 4)

with red curves indicating LOWESS smoother with span = 0.25; Pollen Moisture Index (PMI) derived at Moanatuatua Bog (Jara et al., 2017); PMI derived at Lake Pupuke, Auckland (van den Bos et al., 2018); period of *Agathis australis* expansion at Lake Pupuke (van den Bos et al., 2018); Mean annual Temperature (MAT) derived at Moanatuatua Bog (Jara et al., 2017); MAT derived at Lake Pupuke (van den Bos et al., 2018); Mean Summer Temperature derived at Lake Pupuke (van den Bos et al., 2018); summer insolation at 37 ^{o}C (van den Bos et al., 2018).

Figure 7. Comparison of warm ENSO (El Niño) events record from Lake Pallcacocha, Ecuador (Moy et al., 2002) with a composite Waikato bog humification record derived as the sum of six individual light transmission residuals records from Kopuatai and Moanatuatia bogs (this study), and water table extremes derived from pollen corrosion analysis at Moanatauatua bog (Jara et al., 2017). Vertical green bands indicate extended wet phases in Waikato bogs when summed light transmission residuals are ≥2. Vertical yellow bands indicate extended El Niño phases (manifest in Waikato as dry phases) when warm ENSO events at Lake Palcacocha ≥ 10 per 100 yrs.

For Table Captions - please see file with tables

Supporting Information

Humification correction for mineral content

Peat samples containing mineral (inorganic) matter ('contamination') are likely to affect light transmission readings. The presence of mineral matter lowers the organic proportion of the peat sample resulting in a reduction in the amount of extracted humic acid and hence higher light transmission values. When the environmental factors relating to the peat forming process are the primary consideration, as is the case here, the higher light transmission values for such samples may be misleading. To overcome this problem, Blackford and Chambers (1993) suggested a linear correction for light transmission values on peat samples containing mineral matter, which was subsequently revised by Chambers et al. (2011).

Whilst processing the peat samples in this study, it became evident that enhanced light transmission was occurring as a result of abundant glass shards representing cryptotephra deposits in the stratigraphy and that the effect was non-linear. An experiment was devised to test the relationship between mineral content and light transmission, and to quantify more accurately the effect of highly minerogenic peats on light transmission readings. As a result, we have developed a revised correction procedure based on an exponential relationship between light transmission and mineral 'contamination', to enable the calculation of light transmission values that reflect the peat forming process, independently of mineral matter. We applied this correction in the humification analyses in this study.

Method

Test samples were made using typical *Empodisma*-dominated peat from Kopuatai Bog with a small amount of background mineral content (2.24% from the loss-on-ignition [LOI] measurement). Samples were mixed with fine, dried silica sand (Grade HH) then dried, ground to powder in a Specamill, and thoroughly mixed until homogeneous. Samples of varying proportions of peat and sand were then made and weighed. For each of these samples, three replicates were measured for light transmission, LOI and total organic carbon (TOC). LOI was measured, along with TOC, as this is the standard technique regularly used for determining the organic content of samples in determining their correction equation. Thus, the correction can therefore be applied to either of these indices of organic content.

Results

We found a non-linear relationship between mineral content and light transmission (SI Fig 1).

**SI Fig 1 here*

The results of the experimental data described the exponential curve:

(1) $$\text{light transmission} = 17.855\mathrm{e}^{(0.0171*\text{mineral content})} \quad (\textit{SI Fig 1})$$

From the exponential relationship ($y = a\mathrm{e}^{bx}$) it was then possible to calculate a and b for any given peat sample by solving equations:

(2) $$b = \frac{\ln y_0 - \ln y_e}{x_0 - x_e}$$

(3) $$a = \frac{y_0}{\exp(bx_0)}$$

where: x_0 = the mineral content of the sample,
x_e = 100,
y_0 = the light transmission value of the sample,
and y_e = 100.

Correcting for mineral content could then be done on *any* data point – where a is the corrected light transmission for the sample if it contained no mineral matter.

Results for TOC also showed an exponential relationship with light transmission (SI Fig 2)

**SI Fig 2 here*

To calculate the corrected light transmission for samples on which TOC, not LOI, had been measured, the LOI values would have to be replaced using the relationship between TOC and LOI (SI Fig 3).

**SI Fig 3 here*

These two variables, LOI and TOC, were related linearly ($r^2 = 0.9983$) :

(4) $$\text{mineral content} = 100.47 - 1.7971 \times \text{TOC}$$

Hence, for a TOC measured sample, x_0 in equations (2) and (3) can be replaced such that:

(5) $$b = \frac{\ln y_0 - \ln y_e}{(100.47 - 1.7971x) - x_e}$$

(6) $$a = \frac{y_0}{\exp(b(100.47 - 1.7971x))}$$

These formulae could then be applied to any peat humification light transmission result of known LOI or TOC.

Supporting Information figure captions

Figure SI1. Light transmission plotted against mineral content (calculated from LOI) for experimental samples.

Figure SI2. Light transmission plotted against TOC for experimental samples (note reversal of x axis).

Figure SI3. The relationship between TOC and mineral content (expressed as 100-LOI) for experimental samples.

1442

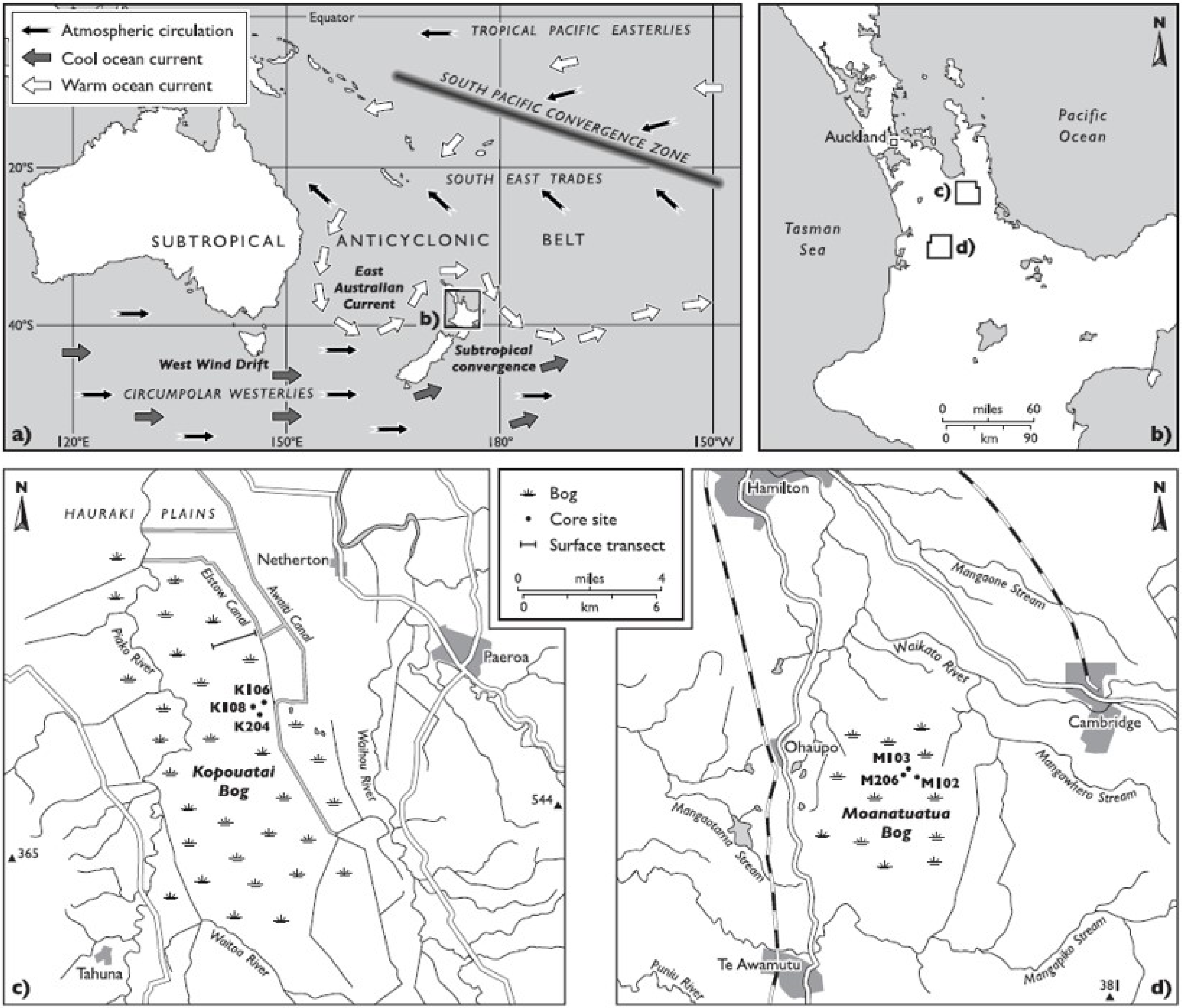

Atmospheric circulation
Cool ocean current
Warm ocean current
Equator
TROPICAL PACIFIC EASTERLIES
SOUTH PACIFIC CONVERGENCE ZONE
SOUTH EAST TRADES
SUBTROPICAL ANTICYCLONIC BELT
East Australian Current
b)
Subtropical convergence
West Wind Drift
CIRCUMPOLAR WESTERLIES
20°S
40°S
120°E
150°E
180°
150°W
a)
N
Auckland
Pacific Ocean
Tasman Sea
c)
d)
0 miles 60
0 km 90
b)
HAURAKI PLAINS
Netherton
Elstow Canal
Awaiti Canal
Piako River
Paeroa
K106
K108
K204
Waihou River
Kopouatai Bog
544
365
Waitoa River
Tahuna
c)
Bog
Core site
Surface transect
0 miles 4
0 km 6
Hamilton
Mangaone Stream
Waikato River
Cambridge
Ohaupo
M103
M206
M102
Mangawhero Stream
Moanatuatua Bog
Mangaotama Stream
Te Awamutu
Puniu River
Mangapiko Stream
381
d)

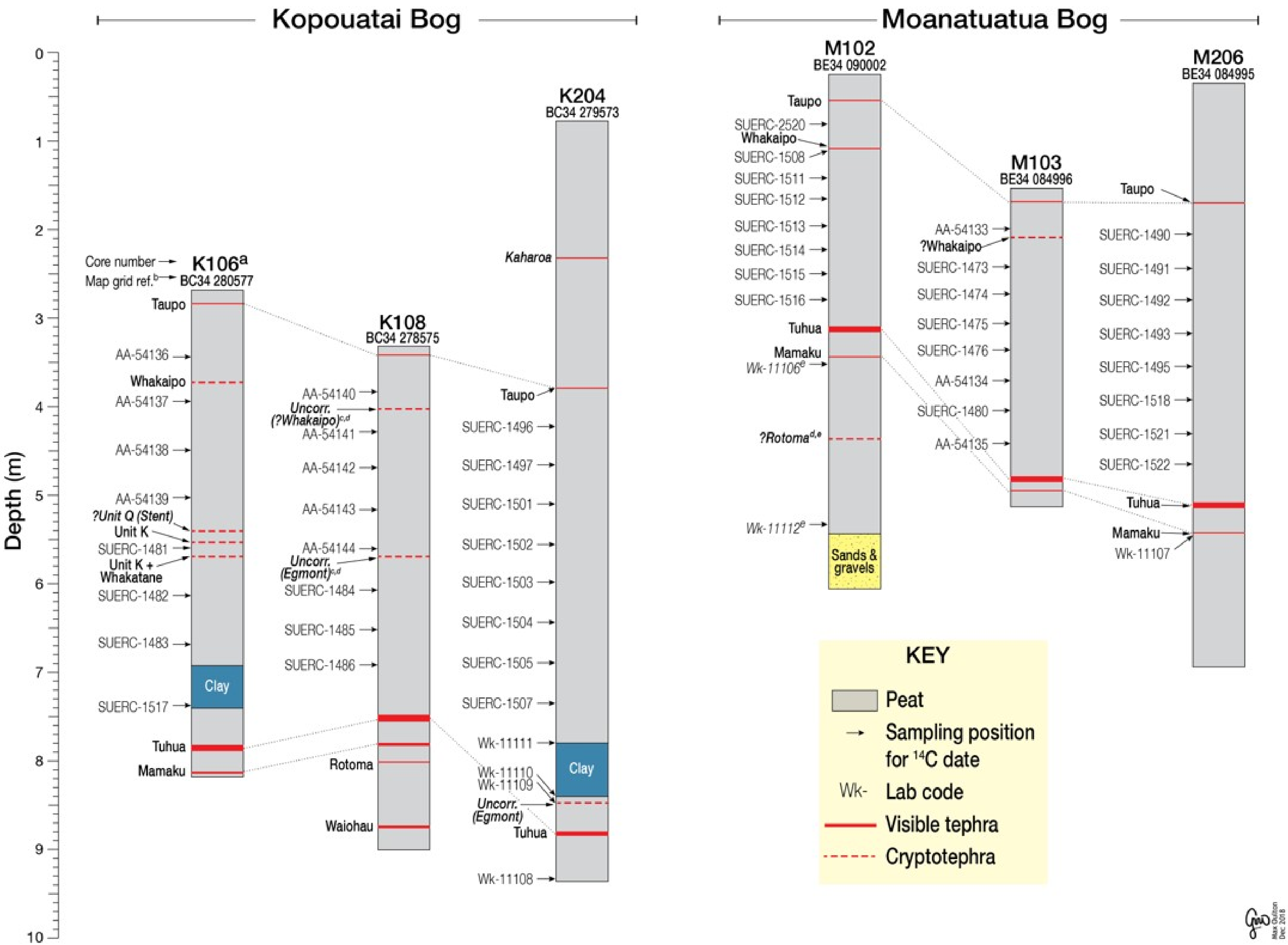

Kopouatai Bog
Moanatuatua Bog
Depth (m)
0
1
2
3
4
5
6
7
8
9
10
Core number
Map grid ref.[b]
K106[a]
BC34 280577
Taupo
AA-54136
Whakaipo
AA-54137
AA-54138
AA-54139
?Unit Q (Stent)
Unit K
SUERC-1481
Unit K + Whakatane
SUERC-1482
SUERC-1483
Clay
SUERC-1517
Tuhua
Mamaku
K108
BC34 278575
AA-54140
Uncorr. (?Whakaipo)[c,d]
AA-54141
AA-54142
AA-54143
AA-54144
Uncorr. (Egmont)[c,d]
SUERC-1484
SUERC-1485
SUERC-1486
Rotoma
Waiohau
K204
BC34 279573
Kaharoa
Taupo
SUERC-1496
SUERC-1497
SUERC-1501
SUERC-1502
SUERC-1503
SUERC-1504
SUERC-1505
SUERC-1507
Wk-11111
Clay
Wk-11110
Wk-11109
Uncorr. (Egmont)
Tuhua
Wk-11108
M102
BE34 090002
Taupo
SUERC-2520
Whakaipo
SUERC-1508
SUERC-1511
SUERC-1512
SUERC-1513
SUERC-1514
SUERC-1515
SUERC-1516
Tuhua
Mamaku
Wk-11106[e]
?Rotoma[d,e]
Wk-11112[e]
Sands & gravels
M103
BE34 084996
AA-54133
?Whakaipo
SUERC-1473
SUERC-1474
SUERC-1475
SUERC-1476
AA-54134
SUERC-1480
AA-54135
M206
BE34 084995
Taupo
SUERC-1490
SUERC-1491
SUERC-1492
SUERC-1493
SUERC-1495
SUERC-1518
SUERC-1521
SUERC-1522
Tuhua
Mamaku
Wk-11107
KEY
Peat
Sampling position for ^{14}C date
Wk- Lab code
Visible tephra
Cryptotephra
Max Oulton Dec 2018

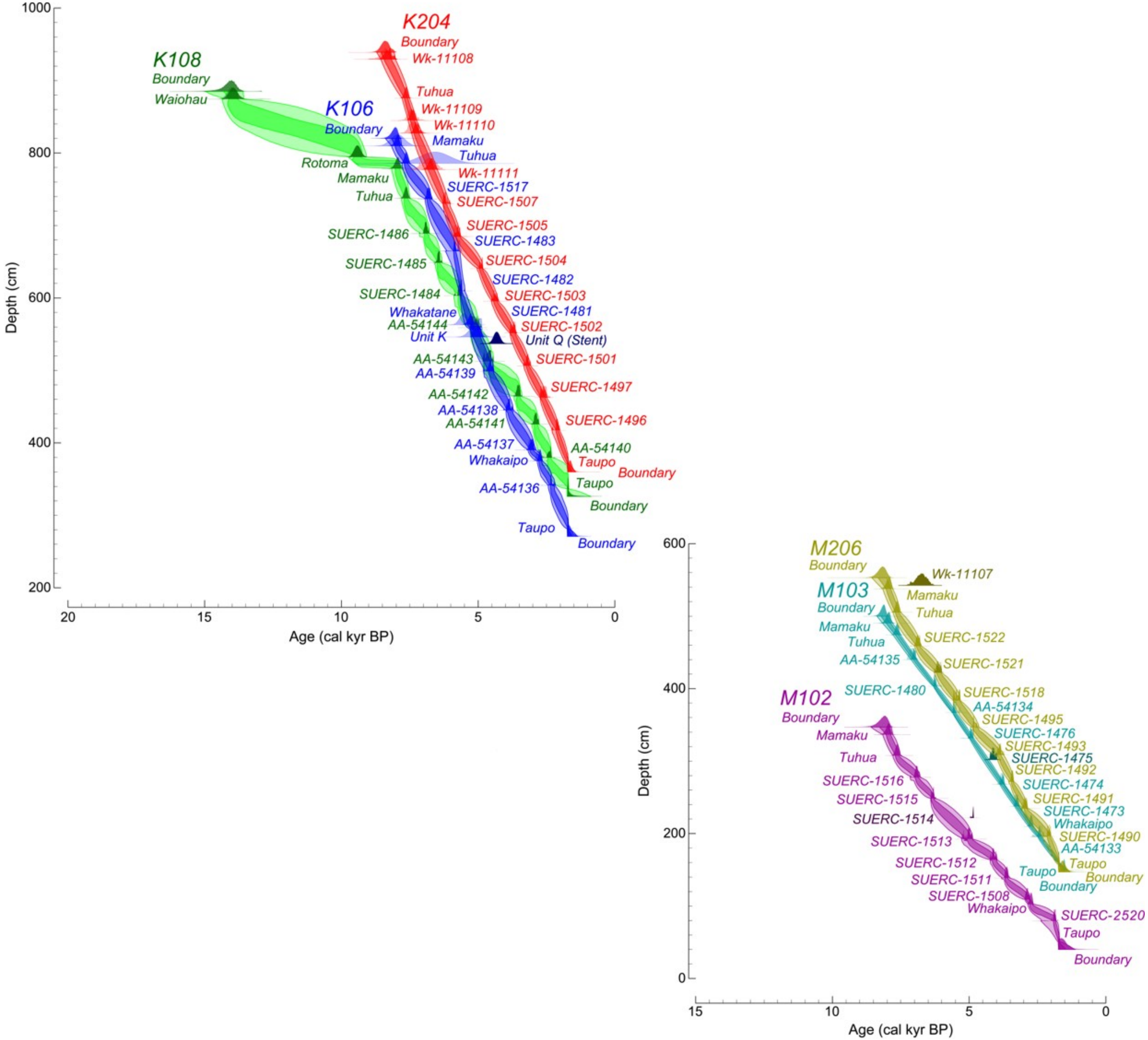

K204
Boundary
Wk-11108
Tuhua
Wk-11109
Wk-11110
Wk-11111
SUERC-1507
SUERC-1505
SUERC-1504
SUERC-1503
SUERC-1502
SUERC-1501
SUERC-1497
SUERC-1496
Taupo
Boundary
K108
Boundary
Waiohau
Rotoma
Mamaku
Tuhua
SUERC-1486
SUERC-1485
SUERC-1484
AA-54144
AA-54143
AA-54142
AA-54141
AA-54140
Taupo
Boundary
K106
Boundary
Mamaku
Tuhua
SUERC-1517
SUERC-1483
SUERC-1482
SUERC-1481
Whakatane
Unit K
Unit Q (Stent)
AA-54139
AA-54138
AA-54137
Whakaipo
AA-54136
Taupo
Boundary
Depth (cm)
1000
800
600
400
200
Age (cal kyr BP)
20
15
10
5
0
M206
Boundary
Wk-11107
Mamaku
Tuhua
SUERC-1522
SUERC-1521
SUERC-1518
SUERC-1495
SUERC-1493
SUERC-1492
SUERC-1491
SUERC-1490
Taupo
Boundary
M103
Boundary
Mamaku
Tuhua
AA-54135
SUERC-1480
AA-54134
SUERC-1476
SUERC-1475
SUERC-1474
SUERC-1473
Whakaipo
AA-54133
Taupo
Boundary
M102
Boundary
Mamaku
Tuhua
SUERC-1516
SUERC-1515
SUERC-1514
SUERC-1513
SUERC-1512
SUERC-1511
SUERC-1508
Whakaipo
SUERC-2520
Taupo
Boundary
Depth (cm)
600
400
200
0
Age (cal kyr BP)
15
10
5
0

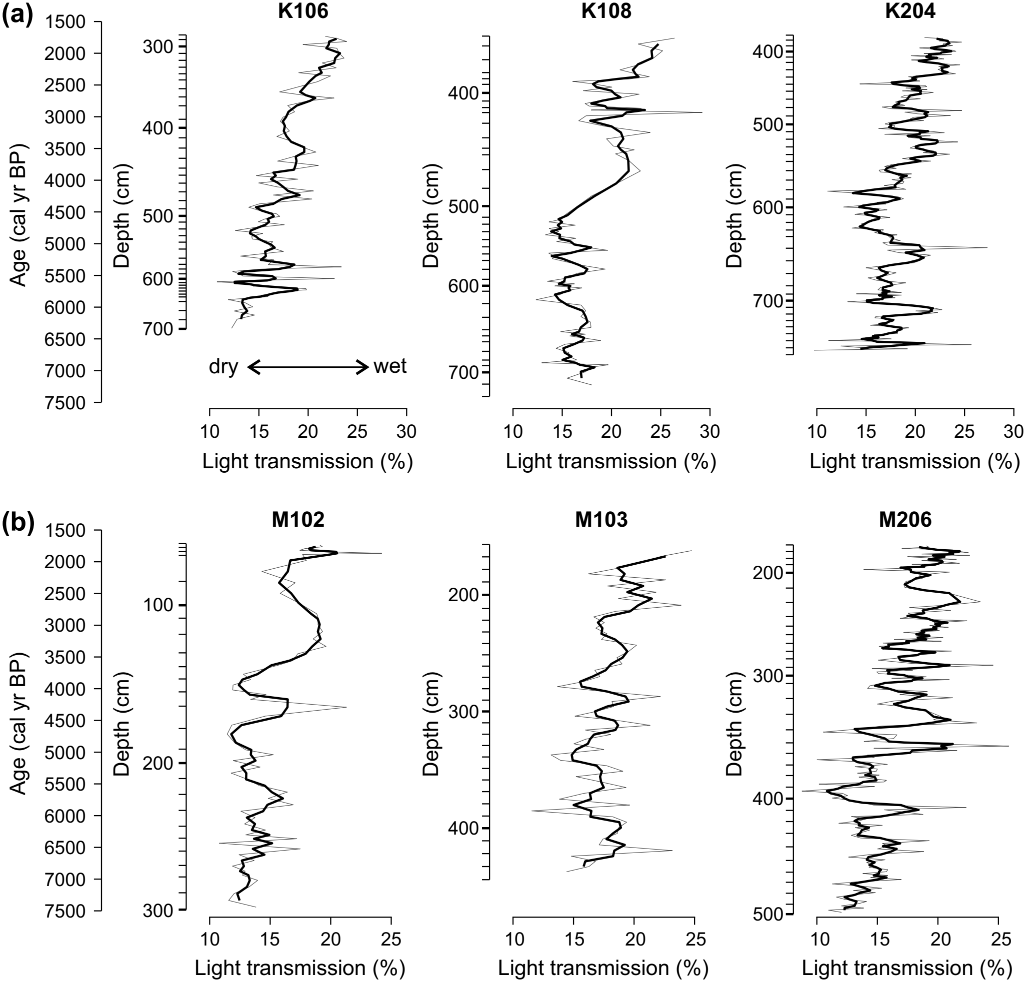

(a)
K106
K108
K204
Age (cal yr BP)
Depth (cm)
dry
wet
Light transmission (%)
(b)
M102
M103
M206

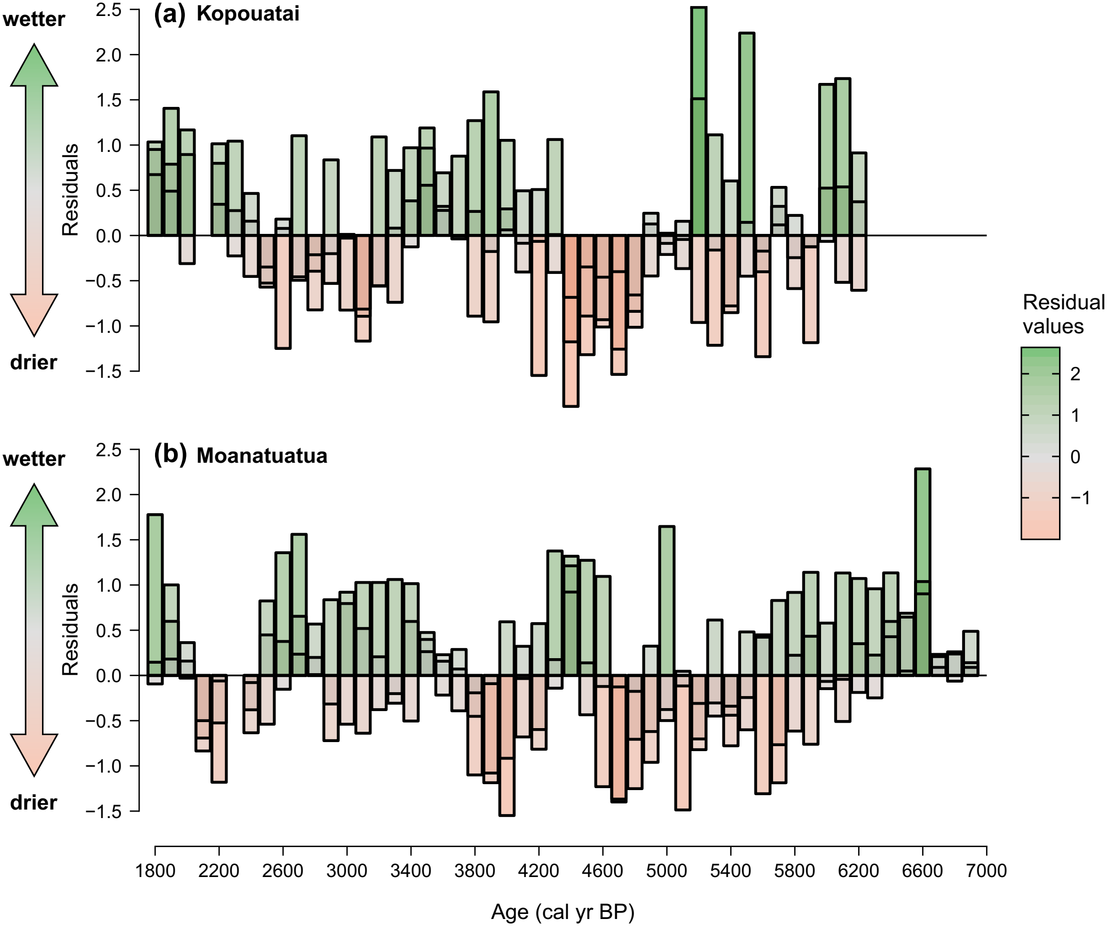

(a) Kopouatai
(b) Moanatuatua
wetter
drier
Residuals
2.5
2.0
1.5
1.0
0.5
0.0
−0.5
−1.0
−1.5
Residual values
2
1
0
−1
1800
2200
2600
3000
3400
3800
4200
4600
5000
5400
5800
6200
6600
7000
Age (cal yr BP)

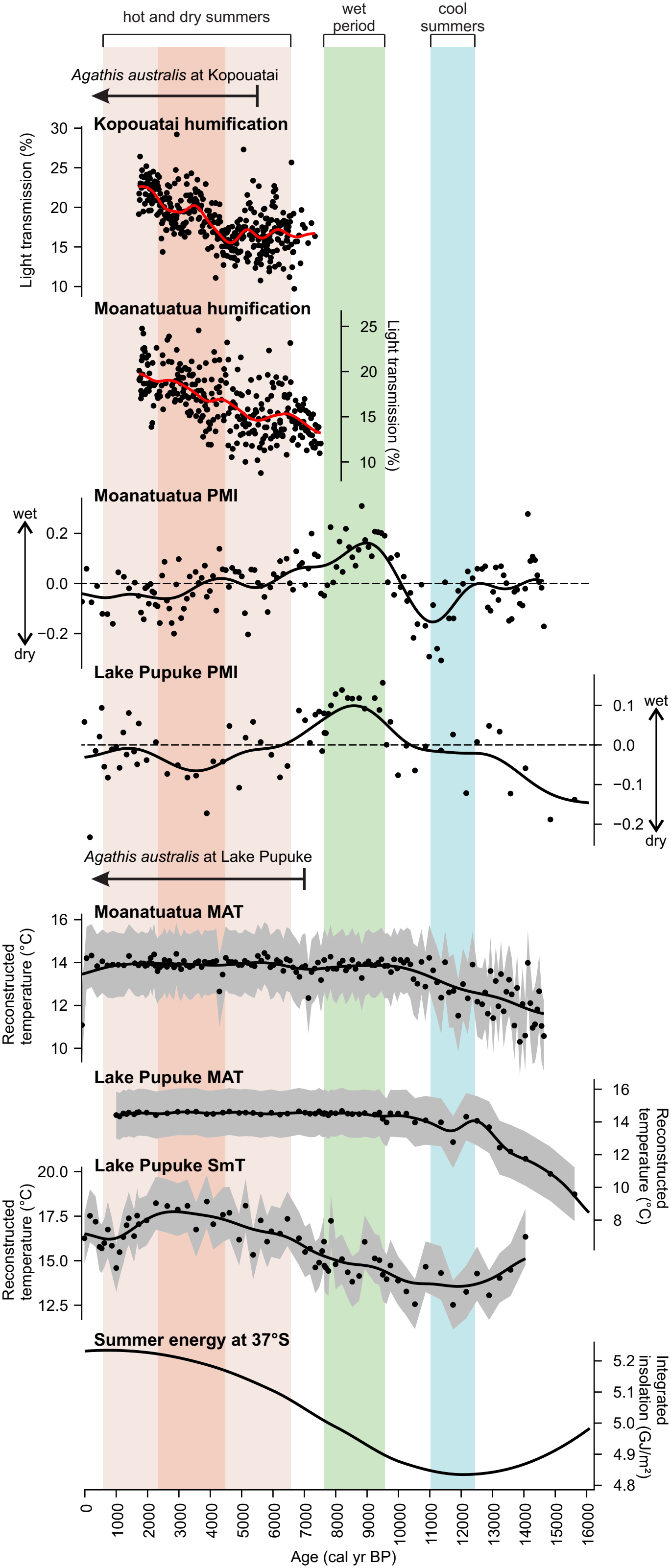

hot and dry summers
wet period
cool summers
Agathis australis at Kopouatai
Kopouatai humification
Light transmission (%)
Moanatuatua humification
Light transmission (%)
Moanatuatua PMI
wet
dry
Lake Pupuke PMI
wet
dry
Agathis australis at Lake Pupuke
Moanatuatua MAT
Reconstructed temperature (°C)
Lake Pupuke MAT
Reconstructed temperature (°C)
Lake Pupuke SmT
Reconstructed temperature (°C)
Summer energy at 37°S
Integrated insolation (GJ/m²)
Age (cal yr BP)

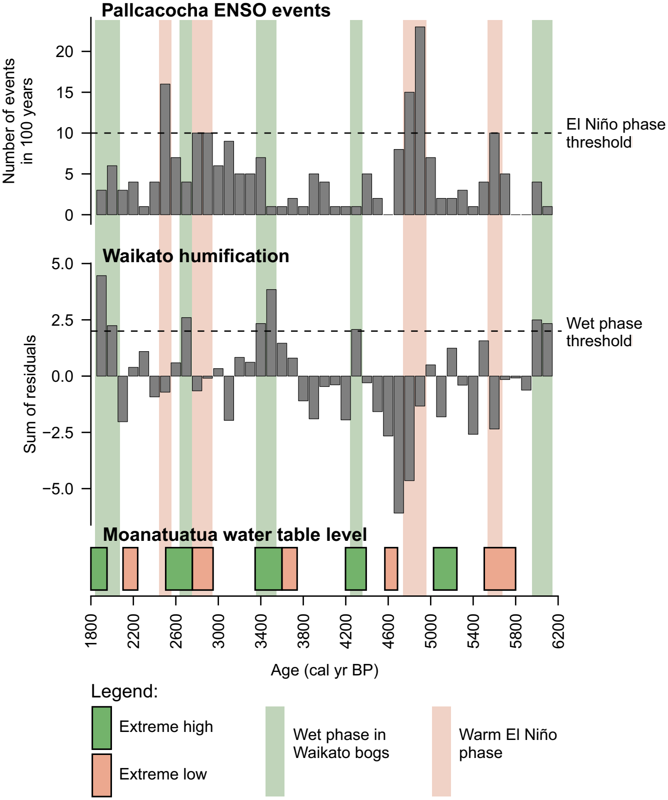

Pallcacocha ENSO events
Number of events in 100 years
El Niño phase threshold
Waikato humification
Sum of residuals
Wet phase threshold
Moanatuatua water table level
Age (cal yr BP)
Legend:
Extreme high
Extreme low
Wet phase in Waikato bogs
Warm El Niño phase

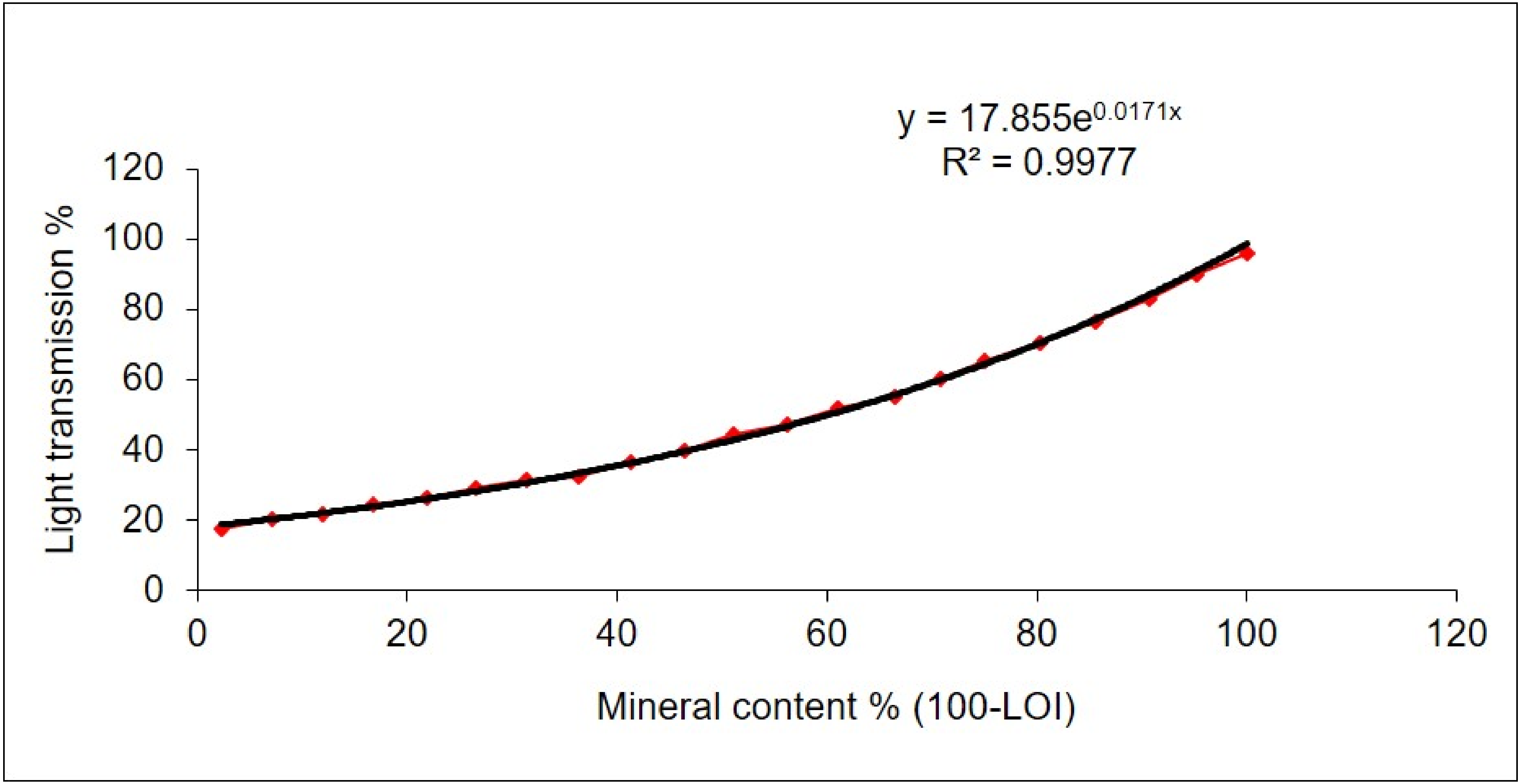
y = 17.855e0.0171x
R² = 0.9977
Light transmission %
120
100
80
60
40
20
0
0
20
40
60
80
100
120
Mineral content % (100-LOI)

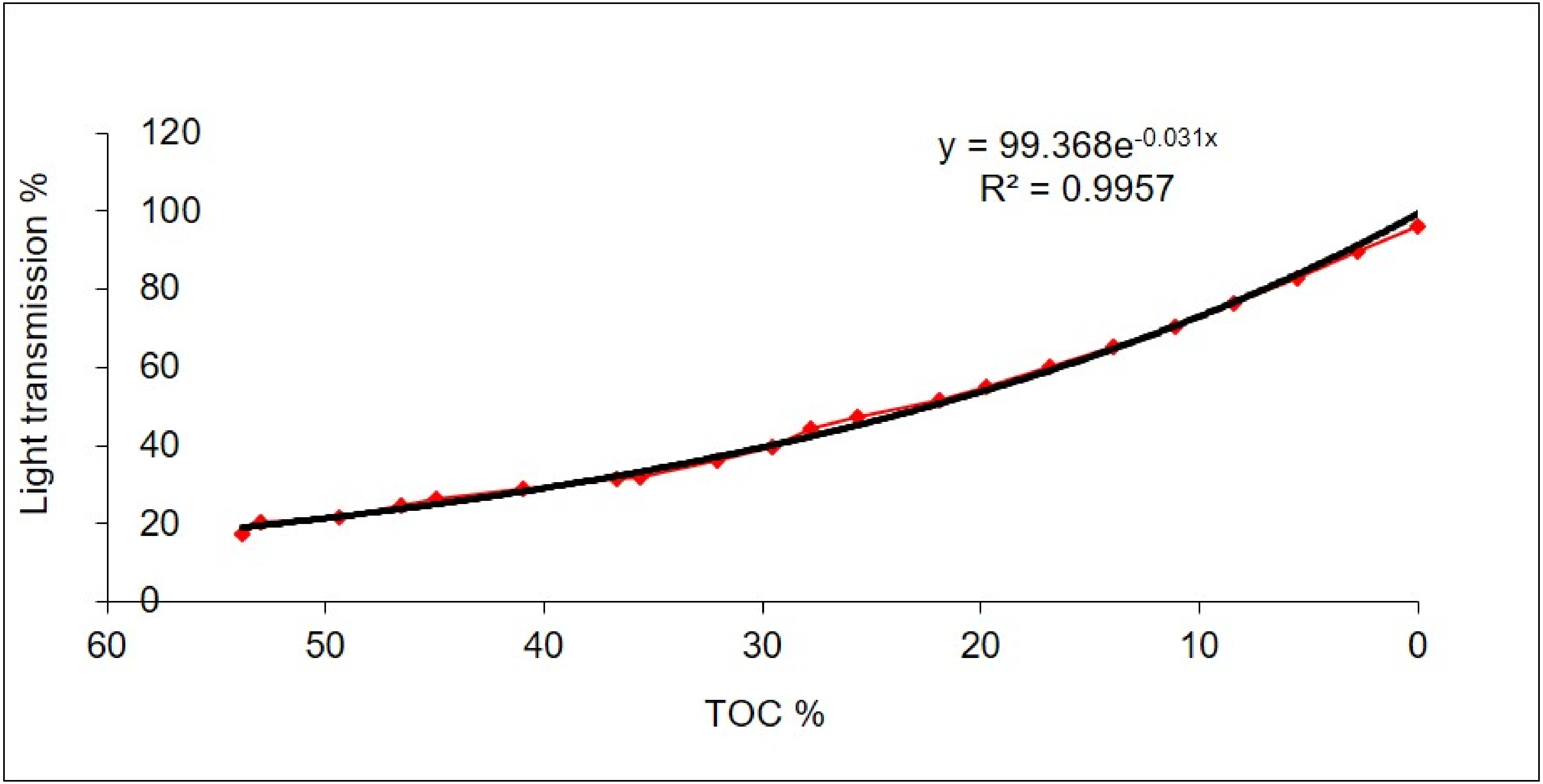

y = 99.368e-0.031x
R² = 0.9957
Light transmission %
120
100
80
60
40
20
0
60
50
40
30
20
10
0
TOC %

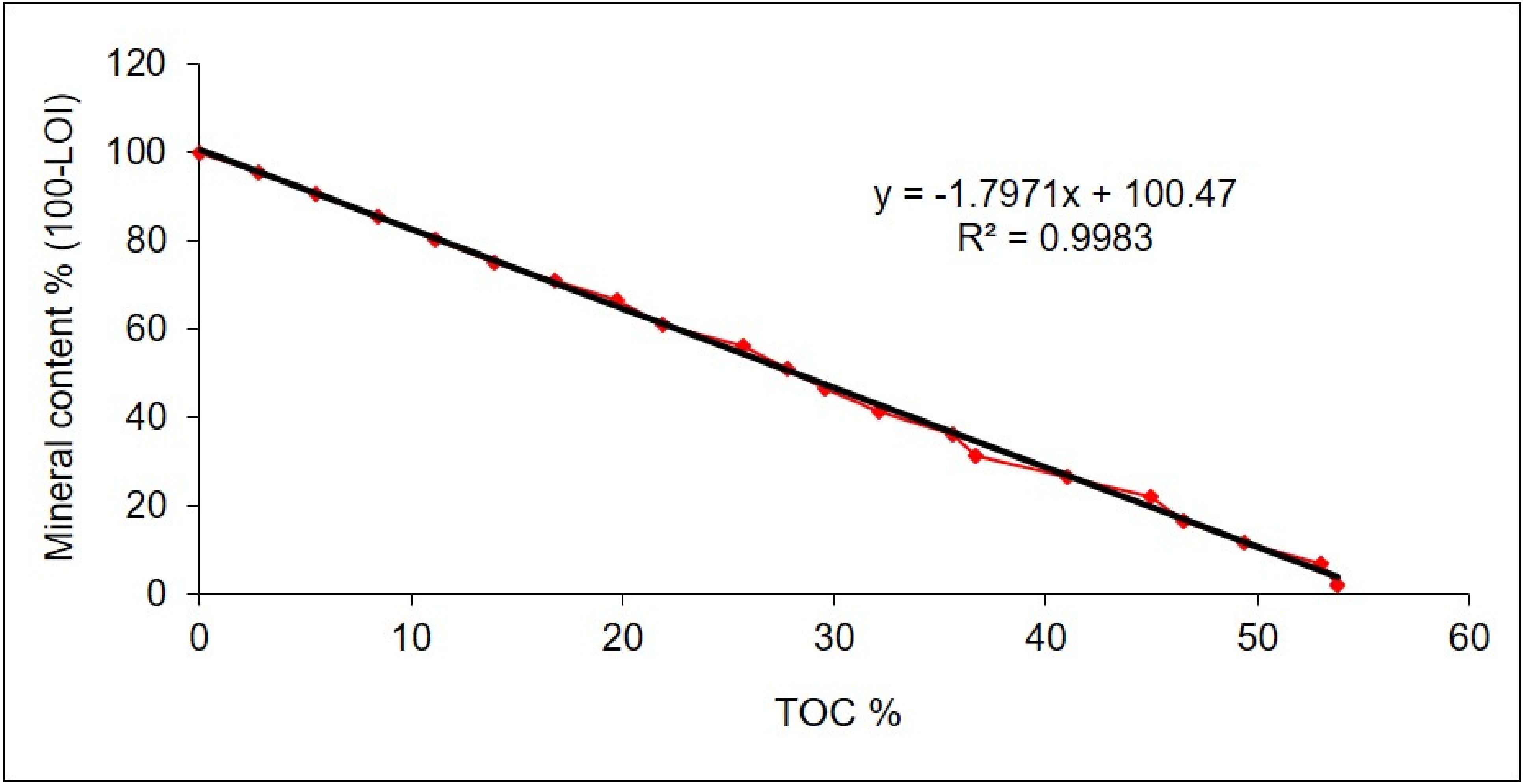

y = -1.7971x + 100.47
R² = 0.9983
Mineral content % (100-LOI)
TOC %
0
20
40
60
80
100
120
0
10
20
30
40
50
60

Table 1. Calendrical ages of visible tephras and cryptotephras in Kopuatai and Moanatuatua bogs

Core	Tephra[a, e]	Depth.min	Depth.max	Depth.ave	Age (± 2σ) cal yr BP	Basis of age[d]	Reference
K106	Taupo	281	282	281.5	1718 ± 10	Dendro	Hogg et al. (2012)
	Whakaipo (ct)	375	375	375	2800 ± 60	Tau bound	Lowe et al. (2013)
	?Unit Q (Stent) (ct)[c]	537	537	537	4322 ± 112	Tau bound	Lowe et al. (2013)
	Unit K (ct)	546	546	546	5088 ± 73	P sequen	Lowe et al. (2013)
	Whakatane[b] (ct)	563	563	563	5542 ± 48	P sequen	Lowe et al. (2013)
	Tuhua	785	786	785.5	7027 ± 170	Tau bound	Lowe et al. (2013)
	Mamaku	809	810	809.5	7992 ± 58	P sequen	Lowe et al. (2013)
K108	Taupo	336	337	336.5	1718 ± 10	Dendro	Hogg et al. (2012)
	Tuhua	737	738	737.5	7027 ± 170	Tau bound	Lowe et al. (2013)
	Mamaku	778	779	778.5	7992 ± 58	P sequen	Lowe et al. (2013)
	Rotoma	794	795	794.5	9472 ± 40	P sequen	Lowe et al. (2013)
	Waiohau	874	875	874.5	14018 ± 91	P sequen	Lowe et al. (2013)
K204	Kaharoa[c]	230	235	232.5	636 ± 12	Dendro	Hogg et al. (2003)
	Taupo	370	371	370.5	1718 ± 10	Dendro	Hogg et al. (2012)
	Tuhua	875	876	875.5	7027 ± 170	Tau bound	Lowe et al. (2013)
M102	Taupo	50	51	50.5	1718 ± 10	Dendro	Hogg et al. (2012)
	Whakaipo	102	103	102.5	2800 ± 60	Tau bound	Lowe et al. (2013)
	Tuhua	307	308	307.5	7027 ± 170	Tau bound	Lowe et al. (2013)
	Mamaku	336	337	336.5	7992 ± 58	P sequen	Lowe et al. (2013)
M103	Taupo	159	160	159.5	1718 ± 10	Dendro	Hogg et al. (2012)
	Whakaipo (ct)	210	210	210	2800 ± 60	Tau bound	Lowe et al. (2013)
	Tuhua	473	475	474	7027 ± 170	Tau bound	Lowe et al. (2013)

	Mamaku	489.5	490.5	490	7992 ± 58	P sequen	Lowe et al. (2013)
M206	Taupo	157	158	157.5	1718 ± 10	Dendro	Hogg et al. (2012)
	Tuhua	500	510	505	7027 ± 170	Tau bound	Lowe et al. (2013)
	Mamaku	537	538	537.5	7992 ± 58	P sequen	Lowe et al. (2013)

[a] See Fig. 2; ct = cryptotephra. Depths in centimetres
[b] Also contained Unit-K glass (Gehrels et al., 2006)
[c] Not used in age modelling here.
[d] Dendro = age based on dendrochronology and wiggle-matching
Tau bound = age modelled using Tau-boundary function of OxCal
P sequen = age modelled using P_sequence function of OxCal
[e] Two uncorrelated Egmont-derived cryptotephras, one aged c. 5.2 cal ka in K108 and one aged c. 7.4 cal ka in K204 (Fig. 2), were not used in age modelling.

Table 2 Electron microprobe analyses[a] of glass shards from tephras/cryptotephras in Kopuatai bog

Tephra[b]	Kaharoa	Taupo (Y)			Whakaipo (V)	Stent (Q) (?)	Unit K	Unit K (5a) and Whakatane (5b)	
Core number	Hodder *et al.* (1991)[e]	Z106 (1a)[f]	Z108	Z204	Z106 (2)[f]	Z106 (3a)[f]	Z106 (4)[f]	Z106 (5a)[f]	(5b)[f]
Depth (m)	2.50-2.52	2.79-2.80	3.36-3.37	3.70-3.71	3.75-3.76	5.37-5.38	5.46-5.47	5.63-5.64	
SiO_2	78.22 (0.31)	75.00 (0.35)	75.86 (0.72)	75.88 (0.83)	76.64 (0.25)	75.81 (0.57)	74.89 (0.76)	75.86 (0.20)	77.52 (0.73)
Al_2O_3	12.49 (0.15)	13.45 (0.20)	13.21 (0.42)	13.40 (0.31)	12.77 (0.25)	13.33 (0.20)	13.01 (0.22)	13.32 (0.10)	12.57 (0.35)
TiO_2	0.13 (0.04)	0.29 (0.06)	0.23 (0.06)	0.25 (0.06)	0.16 (0.03)	0.19 (0.03)	0.21 (0.05)	0.24 (0.05)	0.11 (0.03)
FeO[c]	0.76 (0.26)	2.02 (0.28)	1.82 (0.19)	1.75 (0.28)	1.59 (0.20)	1.79 (0.14)	1.64 (0.24)	1.66 (0.15)	0.90 (0.07)
MnO	na	0.12 (0.05)	0.10 (0.06)	0.08 (0.06)	0.13 (0.02)	0.09 (0.08)	0.09 (0.06)	0.10 (0.10)	0.05 (0.04)
MgO	0.09 (0.13)	0.28 (0.04)	0.24 (0.05)	0.26 (0.05)	0.13 (0.02)	0.18 (0.03)	0.19 (0.03)	0.19 (0.02)	0.10 (0.02)
CaO	0.55 (0.06)	1.49 (0.11)	1.42 (0.18)	1.42 (0.10)	1.02 (0.04)	1.30 (0.10)	1.29 (0.11)	1.25 (0.08)	0.69 (0.06)
Na_2O	3.42 (0.19)	4.37 (0.20)	4.07 (0.14)	3.99 (0.25)	4.28 (0.14)	4.08 (0.43)	4.20 (0.13)	4.25 (0.15)	3.90 (0.15)
K_2O	4.22 (0.43)	2.79 (0.13)	2.88 (0.32)	2.82 (0.11)	3.17 (0.14)	3.08 (0.20)	3.12 (0.21)	2.98 (0.11)	3.98 (0.14)
Cl	0.14 (0.03)	0.18 (0.05)	0.16 (0.03)	0.17 (0.05)	0.16 (0.06)	0.13 (0.03)	0.12 (0.03)	0.16 (0.04)	0.19 (0.05)
Water[d]	0.93 (0.68)	2.95 (1.00)	1.76 (1.62)	4.18 (2.93)	3.10 (1.82)	2.07 (1.43)	1.25 (0.89)	1.97 (0.16)	3.60 (0.98)
n	10	16 (+4)[g]	13 (+1)[g]	13	12	13 (+1)[g]	12	10	8

Table 2 cont

Tephra[b]	Egmont-derived (uncorr)[h]	Tuhua			Mamaku		Rotoma	Waiohau
Core number	Z204	Z106 (6)[f]	Z108	Z204	Z106	Z108	Z108	Z108
Depth (m)	8.42-8.43	7.84-7.85	7.37-7.38	8.75-8.76	8.09-8.10	7.78-7.79	7.94-7.95	8.74-8.75
SiO_2	69.72 (0.82)	74.04 (0.59)	74.60 (0.40)	73.51 (0.98)	78.31 (0.30)	78.06 (0.30)	77.95 (0.07)	77.91 (0.51)
Al_2O_3	15.75 (0.30)	9.53 (0.20)	9.58 (0.20)	9.92 (0.55)	12.28 (0.16)	12.35 (0.21)	12.41 (0.09)	12.62 (0.39)
TiO_2	0.48 (0.06)	0.30 (0.06)	0.26 (0.04)	0.27 (0.08)	0.13 (0.04)	0.12 (0.05)	0.10 (0.00)	0.14 (0.06)
FeO[c]	1.94 (0.29)	5.68 (0.38)	5.44 (0.18)	5.57 (0.29)	0.81 (0.09)	0.88 (0.11)	0.74 (0.02)	0.84 (0.10)
MnO	0.10 (0.05)	0.15 (0.06)	0.15 (0.12)	0.19 (0.07)	0.07 (0.06)	0.06 (0.04)	0.08 (0.01)	0.11 (0.09)
MgO	0.48 (0.13)	0.01 (0.02)	0.02 (0.02)	0.03 (0.05)	0.11 (0.03)	0.11 (0.02)	0.07 (0.02)	0.12 (0.02)
CaO	1.34 (0.19)	0.24 (0.04)	0.24 (0.03)	0.28 (0.18)	0.71 (0.07)	0.72 (0.05)	0.52 (0.03)	0.77 (0.03)
Na_2O	4.62 (0.16)	5.61 (0.27)	5.26 (0.17)	5.64 (0.38)	3.78 (0.15)	3.93 (0.07)	4.03 (0.02)	3.97 (0.15)
K_2O	5.33 (0.12)	4.22 (0.12)	4.20 (0.14)	4.36 (0.14)	3.63 (0.14)	3.61 (0.14)	3.93 (0.06)	3.38 (0.10)
Cl	0.24 (0.04)	0.21 (0.02)	0.25 (0.04)	0.23 (0.03)	0.17 (0.04)	0.15 (0.04)	0.17 (0.03)	0.15 (0.04)
Water[d]	0.92 (1.26)	1.35 (1.22)	0.45 (0.51)	1.78 (1.16)	2.58 (1.24)	2.89 (1.95)	0.36 (0.33)	1.82 (1.29)
n	18	12 (+1)[g]	10	16	13	12	2	13

[a]Means and standard deviations (in parentheses) of *n* analyses (individual glass shards) normalised to 100% loss-free basis (wt%) (Lowe et al., 2017). Analyses by wavelength-dispersive Jeol JXA-733 Superprobe at the Analytical Facility, Victoria University of Wellington, were undertaken by Dr Kathryn Wilson using Smithsonian microbeam glass standards VG-568 and VG-99 (Jarosewich et al., 1980; Jarosewich,

2002) and other reference samples including KN18 (Froggatt, 1983) to correct for machine drift, defocussed beam diameter 20 μm, current 8 nA, and accelerating voltage 15 kV; Na analysed first, no peak search; analyses calculated from 11 x 2 s counts across the peak, curve integrated. na, not available.

[b]Tephra names from Froggatt and Lowe (1990); letters are equivalent volcanological units of Wilson (1993). Stent tephra (Unit Q) defined by Alloway *et al.* (1994).

[c]Total Fe expressed as FeO.

[d]Water by difference from original analytical total.

[e]From Hodder *et al.* (1991, p. 198) (core 22 of Newnham *et al*., 1995).

[f]Analyses from Gehrels *et al.* (2006, p. 178) (numbers in parentheses in column headers refer to their analysis numbers).

[g]Values in parentheses in this line refer to minor subpopulations of different glass composition (not reported here; see Gehrels *et al*., 2006).

[h]This currently-uncorrelated Egmont-derived cryptotephra (c. 7.4 cal. ka) is possibly a correlative of Eg-7 of Lowe (1988) and likely to be a correlative with a unit of the lower part of *Tephra Sequence C* (c. 9.5-6.8 cal. ka) of Damaschke et al. (2017). The Egmont-derived cryptotephra at c. 5.7 m (c. 5.4 cal. ka) in core K108 (no glass analyses) is likely to be a correlative with a unit of the upper part of *Tephra Sequence C* (c. 6-4.3 cal. ka) of Damaschke et al. (2017).

Table 3 Electron microprobe analyses[a] of glass shards from tephras[b] in Moanatuatua bog

Tephra[c]	Taupo (Y)		Whakaipo (V)	Tuhua	Mamaku			
Core number	M103	M206	M102	M102	M102	M103	M203	M206
Depth (m)	1.59-1.60	1.57-1.58	1.02-1.03	3.07-3.08	3.36-3.37	4.90-4.91	3.45-3.46	5.37-5.38
SiO_2	75.47 (0.27)	75.32 (0.69)	77.45 (0.46)	74.63 (0.42)	78.14 (0.46)	78.20 (0.17)	77.52 (0.20)	77.59 (0.37)
Al_2O_3	13.43 (0.10)	13.50 (0.23)	12.40 (0.27)	9.98 (0.61)	12.57 (0.34)	12.36 (0.10)	12.57 (0.18)	12.62 (0.26)
TiO_2	0.26 (0.04)	0.21 (0.09)	0.16 (0.06)	0.27 (0.04)	0.11 (0.05)	0.11 (0.02)	0.11 (0.04)	0.10 (0.03)
FeO[d]	1.94 (0.14)	1.81 (0.17)	1.45 (0.08)	5.40 (0.28)	0.82 (0.08)	0.85 (0.08)	0.88 (0.10)	0.92 (0.17)
MnO	0.12 (0.05)	0.12 (0.10)	0.09 (0.04)	0.14 (0.05)	0.08 (0.04)	0.08 (0.05)	0.06 (0.05)	0.09 (0.06)
MgO	0.27 (0.07)	0.26 (0.11)	0.14 (0.04)	0.02 (0.03)	0.11 (0.03)	0.10 (0.01)	0.14 (0.05)	0.13 (0.08)
CaO	1.49 (0.06)	1.40 (0.15)	0.98 (0.15)	0.23 (0.03)	0.71 (0.06)	0.72 (0.06)	0.75 (0.05)	0.73 (0.10)
Na_2O	4.08 (0.18)	4.32 (0.30)	4.05 (0.22)	4.92 (0.65)	3.70 (0.26)	3.82 (0.15)	3.99 (0.15)	4.00 (0.19)
K_2O	2.77 (0.07)	2.90 (0.15)	3.13 (0.10)	4.16 (0.06)	3.59 (0.11)	3.60 (0.12)	3.81 (0.18)	3.65 (0.18)
Cl	0.17 (0.04)	0.15 (0.03)	0.15 (0.03)	0.24 (0.03)	0.17 (0.04)	0.17 (0.04)	0.16 (0.02)	0.16 (0.03)
Water[e]	0.77 (0.70)	1.88 (1.14)	1.08 (0.48)	0.81 (0.72)	1.46 (1.28)	1.47 (0.94)	1.44 (1.53)	2.25 (1.48)
n	9	16	4	11	11	7	10	16

[a]Means and standard deviations (in parentheses) of *n* analyses (individual glass shards) normalised to 100% loss-free basis (wt%) (Lowe et al., 2017). Analyses were undertaken as described in Table 2.
[b]See also analyses of glass shards of older Waiohau and Rotorua tephras from the base of Moanatuatua bog presented by Jara et al. (2017, their Table S1).
[c]Tephra names from Froggatt and Lowe (1990); letters are equivalent volcanological units of Wilson (1993).

[d]Total Fe as FeO.
[e]Water by difference from original analytical total.

Table 4. AMS and bulk radiocarbon ages from Kopouatai and Moanatuatua bogs and age calibrations.

Core	Lab number[a]	Ave. depth and sample width (cm)	^{14}C age[b] $\pm 1\ \sigma$	$\delta^{13}C$	Unmodelled			Modelled			A_{index}
					95% max	95% min	Mean	95% max	95% min	Mean	
K106	AA-54136	341.5 (1.8)	2347 ± 38	-26.4	2436	2161	2310	2455	2188	2332	114.6
	AA-54137	390.0 (1.0)	2962 ± 38	-29.1	3209	2930	3064	3165	2925	3036	101.6
	AA-54138	445.0 (1.2)	3618 ± 39	-29.8	3984	3719	3873	3975	3721	3855	101.5
	AA-54139	498.8 (1.1)	4116 ± 41	-29.9	4812	4425	4597	4695	4420	4536	107.4
	SUERC-1481	556.2 (1.1)	4433 ± 37	-30.2	5267	4851	4976	5270	4952	5100	54.8
	SUERC-1482	609.5 (1.0)	4925 ± 34	-30.1	5715	5488	5621	5714	5490	5621	103.1
	SUERC-1483	664.5 (2.3)	5039 ± 39	-30.0	5892	5613	5745	5893	5613	5745	
	SUERC-1517	736.6 (1.0)	6017 ± 34	-30.9	6930	6679	6810	6968	6732	6853	88.0
K108	AA-54140	379.7 (1.1)	2404 ± 40	-29.8	2694	2310	2426	2686	2308	2413	104.5
	AA-54141	425.7 (1.0)	2832 ± 37	-29.7	2995	2782	2890	3000	2781	2894	100.7
	AA-54142	464.3 (1.5)	3352 ± 38	-30.2	3679	3446	3537	3681	3446	3537	100.5
	AA-54143	512.7 (1.1)	4145 ± 40	n/a	4821	4447	4642	4817	4445	4628	100.4
	AA-54144	559.2 (1.1)	4514 ± 41	-28.5	5303	4894	5131	5303	4963	5138	102.0
	SUERC-1484	603.1 (2.0)	4999 ± 37	-29.0	5863	5596	5690	5874	5596	5692	100.4
	SUERC-1485	648.7 (2.1)	5707 ± 33	-28.9	6551	6320	6446	6550	6320	6444	100.9
	SUERC-1486	689.0 (2.1)	6101 ± 30	-27.3	7005	6791	6911	7008	6790	6911	100.9
K204	SUERC-1496	417.5 (1.0)	2165 ± 28	-28.6	2299	2010	2116	2299	2017	2129	104.6
	SUERC-1497	462.5 (1.0)	2543 ± 28	-28.8	2741	2458	2591	2736	2497	2622	102.8
	SUERC-1501	506.5 (1.0)	3056 ± 28	-30.7	3340	3076	3208	3331	3076	3199	106.1
	SUERC-1502	551.5 (1.0)	3484 ± 29	-29.3	3829	3610	3710	3833	3629	3727	97.9
	SUERC-1503	595.5 (1.0)	3992 ± 32	-30.7	4520	4256	4398	4514	4250	4376	97.6
	SUERC-1504	640.5 (1.0)	4344 ± 34	-30.2	5026	4825	4880	5033	4827	4902	84.0
	SUERC-1505	684.5 (1.0)	5084 ± 33	n/a	5903	5663	5800	5888	5652	5745	80.7
	SUERC-1507	730.0 (2.0)	5429 ± 31	n/a	6286	6017	6188	6288	6029	6203	108.2
	Wk-11111	777.0 (2.0)	5983 ± 185	-29.1	7252	6399	6798	6948	6495	6721	122.9
	Wk-11110	827.0 (2.0)	6526 ± 174	-30.2	7681	6992	7369	7430	7049	7248	92.0
	Wk-11109	845.0 (2.0)	6571 ± 151	-28.7	7693	7030	7420	7553	7257	7399	120.3
	Wk-11108	929.0 (2.0)	7624 ± 165	-30.1	8857	8014	8401	8549	8024	8295	104.0

Core	Lab no.	Ave. depth and sample width (cm)	^{14}C age $\pm 1\ \sigma$	$\delta^{13}C$	Unmodelled 95% max	Unmodelled 95% min	Unmodelled Mean	Modelled 95% max	Modelled 95% min	Modelled Mean	A_{index}
M102	SUERC-2520	79.5 (1.0)	1962 ± 24	n/a	1928	1755	1867	1928	1755	1867	
	SUERC-1508	109.0 (2.0)	2825 ± 28	-28.0	2960	2785	2880	2958	2792	2882	105.3
	SUERC-1511	138.5 (1.0)	3434 ± 29	-28.2	3816	3515	3639	3717	3515	3628	103.1
	SUERC-1512	164.0 (2.0)	3789 ± 29	n/a	4231	3984	4099	4239	3995	4131	98.4
	SUERC-1513	192.5 (1.0)	4474 ± 29	-27.8	5279	4872	5057	5254	4866	5000	106.3
	SUERC-1514	221.5 (1.0)	4340 ± 27	-28.2	4961	4827	4870	4961	4827	4870	
	SUERC-1515	248.5 (1.0)	5574 ± 29	-28.5	6400	6283	6336	6401	6281	6332	101.7
	SUERC-1516	277.5 (1.0)	6106 ± 36	n/a	7151	6788	6921	7141	6795	6927	106.4
	Wk-11106	348.5 (3.0)	6071 ± 127	-28.3							
	Wk-11112	533.5 (3.0)	9454 ± 206	-28.6							
M103	AA-54133	195.6 (1.2)	2408 ± 38	-28.5	2690	2315	2429	2496	2348	2435	93.9
	SUERC-1473	237.6 (1.2)	3111 ± 28	-29.1	3365	3180	3279	3341	3179	3257	100.3
	SUERC-1474	267.9 (1.4)	3574 ± 32	-28.2	3914	3695	3804	3885	3715	3794	109.4
	SUERC-1475	302.0 (1.0)	3801 ± 33	-27.8	4240	3985	4119	4240	3985	4119	
	SUERC-1476	331.8 (2.3)	4386 ± 35	-29.0	5038	4839	4922	5026	4845	4923	106.2
	AA-54134	366.6 (1.2)	4817 ± 43	-28.4	5600	5327	5499	5603	5472	5548	107.8
	SUERC-1480	403.1 (1.1)	5466 ± 40	-29.1	6306	6025	6222	6301	6189	6251	113.2
	AA-54135	440.0 (1.1)	6240 ± 46	-28.2	7249	6969	7097	7119	6927	7015	84.9

M206	SUERC-1490	196.5 (1.0)	2139 ± 24	-29.0	2149	2008	2075	2300	2009	2122	80.0
	SUERC-1491	234.5 (1.0)	2899 ± 28	-28.5	3075	2865	2973	3058	2863	2948	101.1
	SUERC-1492	271.5 (1.0)	3256 ± 26	-29.4	3555	3364	3433	3548	3364	3431	103.8
	SUERC-1493	308.5 (1.0)	3609 ± 30	-28.3	3974	3724	3860	4065	3733	3895	96.5
	SUERC-1495	346.5 (1.0)	4294 ± 32	-29.0	4875	4630	4800	4873	4629	4786	91.3
	SUERC-1518	383.5 (1.0)	4755 ± 25	-29.3	5581	5323	5441	5580	5323	5438	99.3
	SUERC-1521	422.0 (2.0)	5381 ± 31	-28.1	6268	5997	6115	6269	6000	6124	100.9
	SUERC-1522	458.5 (1.0)	6079 ± 37	-29.0	6999	6753	6882	6980	6751	6868	102.2
	Wk-11107	542.5 (1.0)	5952 ± 152	-28.3	7157	6410	6755	7157	6411	6755	

[a]AA- and SUERC- samples were processed as two separate batches at the NERC Radiocarbon Laboratory (East Kilbride, UK), while Wk- samples were processed at the Waikato Radiocarbon Dating Laboratory (Hamilton, New Zealand). AA- and SUERC- samples were measured using AMS on above-ground plant macrofossils, mainly *Leptospermum scoparium* and *Epacris pauciflora* leaves. Where these were absent, *Epacris* and cf. *Empodisma* seeds and *Gleichenia dicarpa* fronds were used. Wk- samples comprised bulk peat. Age-depth models were developed using OxCal v4.3.2 (Bronk Ramsey, 2009) and the SHCal13 atmospheric curve (Hogg et al., 2013). Each core was modelled with P_Sequence (Bronk Ramsey, 2008) and tephra layers were cross-referenced between cores. Outliers are denoted by missing A_{index} values, "n/a" indicates no result because of insufficient sample, and Wk-11106 and Wk-11112 were sampled from separate cores adjacent to M102. Although not used in this study, these last two dates are included here for completeness.

[b]Conventional radiocarbon ages in ^{14}C year BP ± 1 standard deviation (σ)

Table 5. Pearson correlation coefficients (r) and p-values for correlation between the 100-year bins of humification records for the three Kopouatai and Moanatuatua cores

	K106R	**K108R**
K108R	0.009 (p=0.951)	
K204R	0.329 (p=0.029)*	0.313 (p=0.038)*

	M102R	**M103R**
M103R	0.284 (p=0.043)*	
M206R	0.130 (p=0.365)	0.085 (p=0.552)

* Denotes a significant correlation at the 95% certainty level.